Beta-delayed neutron and gamma-ray spectroscopy of ^{17}C utilizing spin-polarized ^{17}B

H. Ueno,[1, *] H. Miyatake,[2] Y. Yamamoto,[3] S. Tanimoto,[3] T. Shimoda,[3]

N. Aoi,[4] K. Asahi,[5] E. Ideguchi,[4] M. Ishihara,[1] H. Izumi,[3] T. Kishida,[1]

T. Kubo,[1] S. Mitsuoka,[6] Y. Mizoi,[7] M. Notani,[8] H. Ogawa,[5, †]

A. Ozawa,[9] M. Sasaki,[3] T. Shirakura,[3] N. Takahashi,[3] and K. Yoneda[1]

[1]*RIKEN Nishina Center, 2-1 Hirosawa, Wako, Saitama 351-0198, Japan*

[2]*High Energy Accelerator Research Organization*

(KEK), Oho 1-1, Tsukuba, Ibaraki 305-0801, Japan

[3]*Department of Physics, Osaka University,*

Machikaneyama 1-16, Toyonaka, Osaka 560-0034, Japan

[4]*Research Center for Nuclear Physics (RCNP),*

Osaka University, Ibaraki, Osaka 567-0047, Japan

[5]*Department of Physics, Tokyo Institute of Technology,*

2-12-1 Oh-okayama, Meguro-ku, Tokyo 152-8551, Japan

[6]*Japan Atomic Energy Agency, Tokai, Ibaraki 319-1195, Japan*

[7]*Research Center for Physics and Mathematics, Osaka Electro-Communication*

University, 18-8 Hatsucho, Neyagawa, Osaka 572-8530, Japan

[8]*Enrico Fermi Institute, University of Chicago, 5635 S. Ellis Ave., Chicago, IL 60637, USA*

[9]*Institute of Physics, University of Tsukuba, Tsukuba, Ibaraki 305-8571, Japan*

(Dated: February 1, 2013)

Abstract

Excited states in ^{17}C were investigated through the measurement of β-delayed neutrons and γ rays emitted in the β decay of ^{17}B. In the measurement, three negative-parity states and two inconclusive states, were identified in ^{17}C above the neutron threshold energy, and seven γ lines were identified in a β-delayed multiple neutron emission of the ^{17}B β decay. From these transitions, the β-decay scheme of ^{17}B was determined. In particular, a de-excitation 1766-keV γ line from the first excited state of ^{16}C was observed in coincidence with the emitted β-delayed neutrons, and this changes the previously reported β-decay scheme of ^{17}B and level structure of ^{17}C. In the present work, the β-NMR technique is combined with the β-delayed particle measurements using a fragmentation-induced spin-polarized ^{17}B beam. This new scheme allows us to determine the spin parity of β-decay feeding excited states based on the difference in the discrete β-decay asymmetry parameters, provided the states are connected through the Gamow-Teller transition. In this work, $I^{\pi} = 1/2^-$, $3/2^-$, and $(5/2^-)$ are assigned to the observed states at $E_{\mathrm{x}} = 2.71(2)$, $3.93(2)$, and $4.05(2)$ MeV in ^{17}C, respectively.

---

*Electronic address: ueno@riken.jp

†Present Address: National Institute of Advanced Industrial Science and Technology (AIST), Tsukuba Central 2, 1-1-1 Umezono, Tsukuba,Ibaraki 305-8568, Japan

I. INTRODUCTION

Neutron-rich carbon isotopes are attracting because of their anomalous level structures. It has been experimentally shown that none of the odd mass neutron-rich carbon isotopes, $^{15-19}$C, have the ground-state (GS) spin parities of $I^{\pi} = 5/2^{+}$, despite the $d_{5/2}$ valence neutron expected from a naive shell model. In ^{15}C, having the neutron number $N = 9$, the inversion of single-particle levels between $d_{5/2}$ and $s_{1/2}$ is suggested from the GS spin parity of ^{15}C, $I_{\mathrm{GS}}^{\pi} = 1/2^{+}$ [1, 2]. Intriguingly, the further neutron-rich nucleus ^{17}C with $N = 11$, has shown to have $I_{\mathrm{GS}}^{\pi} = 3/2^{+}$. This I_{GS}^{π} assignment was performed through the study of GS properties based on the direct reaction [3–7], β-delayed neutron spectroscopy of the β decay of ^{17}C [8], and magnetic moment of ^{17}C [9]. In the extremely neutron-rich nucleus ^{19}C with $N = 13$, the I_{GS}^{π} value again becomes $1/2^{+}$; this was confirmed and discussed in connection with the formation of a neutron halo [6, 10, 11].

In these neutron-rich carbon isotopes, unlike the valence protons, which occupy the p shell, the valence neutrons occupy the sd shell, where the p-sd cross-shell interactions characteristically play an important role. To gain an understanding of these intriguing properties of p-sd neutron-rich carbon isotopes, it is important to investigate not only the GS but also the structure of the excited states, because those negative-parity states can be described such that one particle in the the p shell of the low-lying positive parity states is excited to the sd shell, and thus, their energy differences from the low-lying positive-parity states are expected to reflect directly such the effective interactions.

With regard to the excited states of ^{17}C, the existence of three low-lying positive-parity states has been proposed at $E_{\mathrm{x}} \sim 210$, 295, and 330 keV below the one-neutron threshold energy $S_{\mathrm{n}} = 0.729(18)$ MeV [12]. An excited state observed at $E_{\mathrm{x}} = 295(20)$ keV [13] in the ^{48}Ca(^{18}O, ^{17}C)^{49}Ti reaction was again observed at $E_{\mathrm{x}} = 295(10)$ for the same reaction, carried out at a slightly higher beam energy [14]. However, the 295-keV state was interpreted to be a background (BG) event during the in-beam γ-ray spectroscopy performed with a ^{17}C beam [15]. Two more excited states were observed at $E_{\mathrm{x}} = 207(15)$ keV and 329(5) keV in the two-step fragmentation reaction [16]. Two corresponding energy levels were observed, i.e., $E_{\mathrm{x}} = 210(4)$ keV and 331(6) keV, in the $p(^{19}$C, ^{17}C$\gamma)$ reaction, for which I^{π} values were assigned as $1/2^{+}$ and $5/2^{+}$, respectively [17]. The same I^{π} assignments were identified in the one-neutron removal reaction of ^{18}C from a proton target, wherein a coupled-channel

analysis was performed for the corresponding levels $E_x = 210$ keV and 330 keV [18], and in the lifetime measurement, in which case the M1 transition strengths were discussed for the observed 212(8)- and 333(10)-keV states [19]. For high-lying states, thirteen positive-parity states, including the $E_x = 310(30)$ keV level, have been observed up to $E_x = 16.3$ MeV in the study of the $^{14}C(^{12}C, {}^{9}C)^{17}C$ reaction [20].

Even then, only a few studies have been conducted on the negative-parity states in ^{17}C. For studying negative-parity states in ^{17}C, it is useful to perform the β-decay study of ^{17}B. In the light mass region of neutron-rich nuclei, the parity of sd-valence neutrons differs from that of p-shell valence protons, whereby β-decay allowed transitions feed negative-parity states [21]. Hence, a β-decay study is useful for studying neutron-rich nuclei located away from the stability line, owing to the large Q_β windows. Over the past several years, a number of such studies have been performed on the structure of light-mass neutron-rich nuclei through the time-of-flight (TOF) measurement of emitted β-delayed neutrons [8, 22–25].

In the present work, we performed the spectroscopic study of β-delayed neutrons and γ rays in the β decay of ^{17}B in order to investigate the level structure of ^{17}C (hereafter, β-delayed neutron(s) and β-delayed γ ray(s) are denoted as β-n and β-γ, respectively). The β-n measurement of the ^{17}B β decay has thus far been reported in Ref. [24], and in this study, several β-decay transitions to the excited states in ^{17}C above the neutron threshold energy, which were followed by neutron emission, were observed. However, in the construction of the decay scheme, all transitions observed in a one-neutron (1n) emission channel were assumed to be directly connected to the GS of ^{16}C. In order to identify the final states in ^{16}C subsequent to the β-n emissions, we also conducted γ-ray measurements in coincidence with the β rays and neutrons. Moreover, it should be noted that this measurement was combined with a technique of fragmentation-induced spin-polarization [26, 27]. Thus, the GS of ^{17}B, as an initial state of β decay, was spin-polarized. The angular distribution of the β decay through the Gamow-Teller (GT) transition from a spin-polarized nucleus is known to show anisotropy with respect to the polarization axis, and it is characterized by $A_\beta P$, where A_β denotes the asymmetry parameter of the corresponding GT transition given by the I^π value of the initial and final states and P denotes the polarization of the parent nucleus. Since P is common to all the transitions, the final state I^π can be assigned such that A_β becomes proportional to the experimentally determined $A_\beta P$ values when the initial state

I^π is known. For the first time, by using this new method, the I^π values of the excited states in ^{15}C have been successfully assigned with the spin-polarized ^{15}B beam [28]. Further, by taking the advantage of highly spin-polarized Li and Na beams, the nuclear structures of ^{11}Be [29] and ^{28}Mg [30] have been studied through the spin-parity assignment of the excited states.

II. EXPERIMENTAL PROCEDURE

A. Production of spin-polarized ^{17}B beam

A spin-polarized ^{17}B beam was produced using the same procedure as described in Ref. [31], in which the fragmentation-induced spin polarization technique was adopted [26, 27]. A beam of ^{17}B was obtained from the fragmentation of a ^{22}Ne projectile with an energy of $E/A = 110$ MeV and a current of 90 particle-nA incident on a ^{93}Nb target having a thickness of 1.07 g/cm^2. In order to obtain a spin-polarized ^{17}B beam, the emission angles and outgoing momenta of the ^{17}B fragments were suitably selected [26, 27]. Thus, fragments emitted within radial angles $\theta_{\rm L} = 1.5° - 5.0°$ and azimuthal angles $|\phi_{\rm L}| \leq 2.0°$ along with the primary beam were accepted by the RIKEN projectile-fragment separator RIPS [32], using a beam swinger installed upstream of the target. A range of the momentum values, i.e., $p = 7.11$ to 7.55 GeV/c, was selected with the help of a slit at the intermediate momentum-dispersive focal plane. This momentum range corresponds to the range $1.01p_0$–$1.07p_0$, where $p_0 = 7.03$ GeV/c is the fragment momentum corresponding to the projectile velocity. The isotope separation was given by the combined analyses of the magnetic rigidity and the momentum loss in a wedge-shaped degrader [32] with a median thickness of 1638 mg/cm^2 and a slope angle of 8.67 mrad.

The spin-polarized and isotope-separated ^{17}B fragments were then introduced into an apparatus located at the final focus of RIPS, for the β-delayed particle measurement. They were implanted in a Pt stopper located at the center of the apparatus, which consisted of a stack of four 100-μm-thick Pt plates. The beam implantation was confirmed with plastic scintillators placed upstream and downstream of the Pt stopper. The the upstream counter was used to distinguish the $Z > 4$ beam particles from contaminating tritons. Under the conditions described above, RIPS provided a ^{17}B beam with a purity of $\sim 100\%$, not

considering tritons, and an intensity of 17.3 particles per second (pps).

B. Detector apparatus

We combined the β-ray detected nuclear magnetic resonance (β-NMR) technique [33] with the β-delayed particle emission measurement. A static magnetic field, $B_0 = 50.0$ mT, whose inhomogeneity was $\Delta B_0 / B_0 \leq 10^{-2}$, was applied to the Pt stopper with a Helmholtz-type air coil in order to preserve the spin polarization of ^{17}B. The effective diameter of the coil was $\phi = 250$ mm. β-Rays emitted from the implanted fragments were detected with β-ray telescopes, consisting of two plastic scintillators, located above and below the Pt stopper. To exclude BG events, such as those involving cosmic muons, coincidences with signals from the other side of the β-ray telescope were checked as soon as a β-ray was detected.

The β-n emitted from the implanted ^{17}B were measured with a high-energy neutron detector array [25, 28], consisting of a set of twelve plastic scintillators, whose shapes were curved in the vertical direction with a 150-cm radius, 160-cm arc length, and 40-cm latitudinal width in the median plane. The achieved electron-equivalent threshold energy, $E_{\text{th}} = 3.4(27)$ keVee, of the neutron detector array, enabled the detection of low-energy neutrons at $E_{\text{n}} \sim 0.5$ MeV, and an efficiency of 5.6% for $\sim$1 MeV neutrons was achieved as a result. A high-energy neutron detector array was placed 1.5 m away from the Pt stopper, as shown in Fig. 1, covering the solid angles $\Omega_{\text{n}} = 0.21 \times 4\pi$ sr. In this configuration, neutrons emitted vertical to the β-ray direction were detected, which minimized the neutron-energy broadening due to β-ray recoil effects. The neutron energies were determined using the TOF method, wherein the β-ray signal was used as the start pulse. The signal was read out from photomultiplier tubes (PMTs) attached at each end, and both the read out signals were used to determine the correct TOF by calculating the mean time. Neutrons within the energy range $E_{\text{n}} = 0.5 \sim 10$ MeV were analyzed with this high-energy neutron detector array.

The detection efficiency of the neutron detector array was determined using ^{15}B and ^{17}N beams, whose β-decay branches associated with β-n emission are known [22, 34]. Using these calibration data, the efficiency was determined as a function of the energy E_{n}, based on the simulation code given in Ref. [35], where the reduction of photo-propagation in the plastic scintillator was taken into account. Details pertaining to the high-energy neutron detector array are given in Ref. [28]. For the measurement of neutrons having an energy

down to $E_n \gtrsim 0.01$ MeV, a low-energy neutron detector array [25] covering the solid angle $\Omega_n = 0.037 \times 4\pi$ sr was placed on a concentric circle to achieve a distance of 0.5 m from the Pt stopper, which consisted of a set of ten 45 mm × 25 mm × 300 mm plastic scintillators. The signal was read out from the PMTs attached at each end. The threshold energy was set to 2 keVee using the Compton edge of ^{137}Cs.

In addition to the neutron counters, a 50 mm$^{\phi}$ × 70 mm Clover Ge detector [36] and a set of four 80 mm × 80 mm × 152 mm NaI(Tl) detectors were placed above and below the β-ray telescope, as shown in Fig. 2. The PMTs housed in the NaI(Tl) detectors are a type of fine-mesh dynodes, which can be operated under strong magnetic fields with strengths of over 1 T [37]. In front of each Ge and NaI(Tl) detector, 2-mm-thick plastic scintillators were placed in order to distinguish γ and β rays. With the help of these plastic scintillators, NaI(Tl) detectors were used to measure not only γ-ray energies but also the β-ray total energy, E_β, for up to 30 MeV, which covers a $Q_\beta(^{17}$B$)$ of 22.68(14) MeV [12]. The E_β data were calibrated for a sufficiently wide range using ^{17}N and ^{15}B, whose Q_β values are 8.680(15) and 19.094(22) MeV, respectively [12].

C. Block diagram

The conventional block diagram for β-NMR measurements shows a beam being pulsed with a beam bombardment period of T_B. At the beginning of the beam-off period in these measurements, the oscillating magnetic field B_1 is applied for a duration of T_R, with its frequency swept over a Larmor frequency in order to reverse the direction of the spin polarization by means of the adiabatic fast passage (AFP) NMR method [38]. Then, β rays are counted during the following period, T_C. This unit cycle, $T_B + T_R + T_C$, is repeated many times until sufficient statistics have been accumulated. Note that the time length of the unit cycle is generally set to $2/\lambda$, where λ is the decay constant of the nuclei of interest. Through the execution of this sequence, a maximum figure of merit given by $Y_\beta \times P^2$ is achieved, where Y_β is the β-ray counting rate and P is the nuclear spin polarization. Ideally, T_B should be set by taking into account the spin-lattice relaxation time of the nuclei. The β-ray counting rate Y_β is then given by

$$Y_\beta = \frac{I_B e^{-\lambda T_R}(1 - e^{-\lambda T_B})(1 - e^{-\lambda T_C})}{\lambda(T_B + T_C + T_R)(1 - e^{-\lambda(T_R + T_C)})},$$
(1)

where I_B is the beam-implantation rate during the period T_B. In this sequence, however, ~50% of the beam needs to be blocked, despite the low production yield of the ^{17}B beam.

For more efficient measurements, the block diagram was improved in the present study, and it is illustrated in Fig. 3. The beam was not pulsed periodically at fixed durations. Instead, as soon as a ^{17}B particle was identified by the beam-line counters equipped with RIPS, the beam bombardment was turned off for 19.5 ms. At the beginning of the beam-off period, the B_1 field $\simeq 1.6$ mT was applied for a duration of $T_R = 1.5$ ms, and in this duration, the frequency of B_1 was swept over the Larmor frequency ν_0 of ^{17}B [31] in the frequency window $\Delta\nu/\nu_0 = 2\%$. Then, the β rays, in addition to γ rays and neutrons, were measured during a subsequent time period of $T_C = 18$ ms. After the beam-off period, the beam bombardment was again turned on until the next ^{17}B particle was detected. The B_1 field was applied every two beam-off cycles, to ensure that the direction of the spin polarization would change alternately; this reduced the systematic error due to differences in the efficiencies of the two β-ray telescopes and long-term beam-profile fluctuation. The Y_β yield in this *beam-waiting* mode is given by

$$Y_\beta = \frac{I_B \left(e^{-\lambda T_R} - e^{-\lambda(T_R + T_C)}\right)}{1 + I_B(T_R + T_C)}. \tag{2}$$

Based on Eqs. (1) and (2), the yields of ^{17}B Y_β were calculated, for the purpose of comparison, as a function of the intensity of a ^{17}B beam in the fixed beam-on/off cycle mode and the *beam-waiting* mode, where $(T_B, T_R, T_C) = (7.3, 1.5, 7.3)$ ms was assumed as a typical sequence in the former mode. As shown in the inset of Fig. 3, $Y_\beta = 9.6$ counts per second (cps) for the *beam-waiting* mode, and it is 2.6 times larger than $Y_\beta = 3.6$ cps, which is observed for the fixed beam-on/off cycle mode under an actual ^{17}B intensity of $I_B = 17.3$ pps. Factually, 12.9-pps ^{17}B particles were implanted at the intensity of $I_B = 17.3$ pps because of the dead time due to the 19.5-ms beam blocking period $T_R + T_C$. This effect is already considered in Eq. (2).

Another important advantage of the new *beam-waiting* mode is the high S/N ratio in the β-ray measurements. Given the reported multiple neutron emission probabilities in the ^{17}B β decay [39], 3.6 β rays are emitted on an average in the β-decay chain initiated by one ^{17}B β decay. Since all decay-chain nuclei have significantly longer lifetimes than ^{17}B, the BG β rays from these nuclei are assumed to be detected with the same probability inside T_C windows. For $I_B = 17.3$ pps, the S/N ratio in the fixed beam-on/off mode is S(3.6 cps)/N(16.8 cps)

= 0.22, whereas in the *beam-waiting* mode, the S/N ratio is 4.3 times better and has the value S(9.6 cps)/N(10.5 cps) = 0.92.

D. Principle of the spin parity assignment

The angular distribution function $W(\theta)$ for the β rays emitted from ^{17}B with the spin polarization P is given by

$$W(\theta) \propto 1 + (v/c)A_\beta P \cos\theta \tag{3}$$

where θ denotes the angle between the direction of the β emission and the axis of the nuclear polarization, v and c are the velocities of the β particles and light, respectively, and A_β is the asymmetry parameter. For simplicity, we use the approximation $v/c \simeq 1$, since only a high-energy portion of the β spectrum is included in the analysis. Then, the asymmetry $A_\beta P$ of the β-decay transition feeding neutron emissions is given by

$$A_\beta P = \frac{\sqrt{\rho} - 1}{\sqrt{\rho} + 1}. \tag{4}$$

Here, using the measured β-n spectra recorded with the identification of the signal-detected β-ray telescope, the double ratio ρ in Eq. (4) is given by

$$\rho = \left(\frac{N_U}{N_D}\right) \bigg/ \left(\frac{N_U^*}{N_D^*}\right), \tag{5}$$

where $N_{U,D}$ are the relevant peak counting rates in the neutron TOF spectra measured in coincidence with signals from the β-ray telescopes located above (denoted by U) and below (denoted by D) the Pt stopper and $N_{U,D}^*$ are those obtained with the resonant B_1-field application. With the obtained $A_\beta P$ values, asymmetry parameters A_β can be determined provided the polarization P is known.

In the case that the spin I_i state decays through the pure GT $\beta^\mp$-decay transitions associated with the spin change ΔI, the β-decay asymmetry parameter A_β value is given by

$$A_\beta = \begin{cases} \mp 1 & (\Delta I = -1) \\ \mp 1/(I_i + 1) & (\Delta I = 0) \\ \pm I_i/(I_i + 1) & (\Delta I = +1) \end{cases} . \tag{6}$$

By comparing the determined A_β values to the value given in Eq. (6), the final spin parity I_f^π can be determined in the case of a pure GT β-decay.

In order to apply this method, it is necessary to know I_i^π and one I_f^π value from among the GT β-decay transitions for the determination of the spin polarization P. In the present experiment, $I_i^\pi = 3/2^-$ is known for the GS of ^{17}B [31], whereas none of the final state I_f^π values are known. Therefore, similar to the I^π assignment for ^{15}C [28], the following method was performed.

For a given set of GT transitions to the level I_f^j (j=1, 2, $\cdots$, n), there are 3^n combinations of the possible A_β values. For each allocated $A_{\beta j}$ value, the polarization is evaluated as $P_j = (A_\beta P)_j / A_{\beta j}$, where $A_\beta P_j$ is the measured asymmetry. For the proper combination of A_β values, i.e., for the correct spin assignments for all relevant final states, the evaluated P_j values need to be consistent with each other. It is therefore expected that for improper combinations of A_β values, the expected value of P will have systematic errors and the variance of P will increase. In other words, a correct assignment should reveal the least variance of P. This is the guiding principle for determining I_f^π values simultaneously. For the ith set of $A_{\beta j}$ values, the mean spin polarization $\bar{P}_i$ is calculated as

$$\bar{P}_i = \frac{\sum_j P_j w_j}{\sum_j w_j} p \tag{7}$$

where w_j is the statistical weight factor for each P_j value,

$$w_j = \frac{A_{\beta j}^2}{\sigma_{(A_\beta P)_j}^2} \tag{8}$$

with the experimental error $\sigma_{(A_\beta P)_j}$ for $(A_\beta P)_j$. By definition, the reduced χ_ν^2 for the ith set is given as

$$\chi_\nu^2(\bar{P}_i) = \frac{1}{\nu} \sum_j (P_j - \bar{P}_i)^2 w_j \quad (i = 1, \ 2, \cdots, \ 3^n) \tag{9}$$

where ν denotes the degree of freedom ($\nu = n - 1$). The above-mentioned guiding principle is that the most probable set of $A_{\beta j}$ values should yield the least χ_ν^2 among the 3^n values for all possible combinations of $A_{\beta j}$ values. In such a case, $\bar{P}_i$ can be regarded as the statistically expected spin polarization P, whose error is defined by

$$\sigma_{\bar{P}_i} = \frac{\sum_j (\bar{P}_i - P_j)^2 w_j}{\sum_j w_j}. \tag{10}$$

III. ANALYSIS AND RESULTS

The ^{17}B nucleus has the ground-state spin parity $I^\pi = 3/2^-$. Its β decay, whose halflife is $t_{1/2} = 5.08(5)$ ms and Q_β is 22.68(14) MeV [12], can be characterized by a β-delayed multiple neutron emission [39, 40], for which multiplicities M_n of up to four have been reported [39]. In the following analysis, the decay property was investigated by classifying the multiplicity of the emitted β-n.

A. 0n-decay branches

The 0n mode of the ^{17}B β decay, i.e., a β decay not followed by β-n emission, can feed excited states in ^{17}C below the neutron separation energy $S_n = 0.729(18)$ MeV or the GS. Until now, the existence of three excited states has been suggested at the excitation energy values $E_x \sim 210$ keV [16–19], 295 keV [13, 14], and 331 keV [16–20], below $S_n = 0.729(18)$ MeV. Investigation of these three states is a central subject for the 0n channel.

1. γ-Ray energy spectra obtained from the β-γ coincidence measurements

The observed γ-ray energy peaks below $S_n = 0.729(18)$ MeV, measured with the Ge detector in coincidence with the β ray from ^{17}B, are summarized in Table I. For a comparison, details of γ rays observed in a BG measurement without a beam and in a detector-calibration measurement with a ^{17}N beam are also listed in Table I. First, the γ rays observed in the BG measurement, i.e., $E_\gamma = 77(2)$, 242(1), 352(1), and 609(2) keV, as well as the 511-keV annihilation γ ray, can be excluded from the ^{17}B β-γ candidates. They can be assigned to KX or the γ rays from the lead parts of the experimental setup, in which some amount of the U/Th decay-chain isotopes ^{214}Pb and ^{214}Bi are considered to be included. The reason that the 242(1)-keV γ ray was not observed in the ^{17}N measurement is not clear. This may be attributable to the short measurement time. Next, the γ rays observed in the ^{17}N β-γ measurement, i.e., $E_\gamma = 596(5)$ and 696(8), can be also excluded. They originate from the (n, γ) or (n, n'γ) reactions, given that their shapes are broadened and skewed towards higher energy, which is a typical feature that reveals the neutron-recoil effect in Ge detectors. Here, a 67(1)-keV peak observed in both the ^{17}B and the ^{17}N measurements can be assigned to the KX$_{\alpha 1}$ rays originating from the Pt stopper excited by the β rays. The remaining γ-ray

11

peaks at 295(2) and 331(2) keV, as well as a small peak at $E_\gamma = 217(2)$ keV, are thus the potential γ rays emitted from ^{17}C subsequent to the ^{17}B β decay.

2. *Properties of the peaks at $E_\gamma = 217$, 295, and 331 keV*

Properties of these γ rays were then investigated in terms of the total energy of the feeding β ray, which was measured with the set of NaI(Tl) detectors and 2-mm-thick plastic scintillators described in Sec. II B. The de-excitation γ rays from low-lying excited states of ^{17}C are associated with large β-ray energies, where the maximum β-ray energies are $E_\beta^{\text{max}} \geq Q_\beta - S_{\text{n}} \simeq 22$ MeV, owing to the small S_{n} value. Thus, an E_γ spectrum was obtained, as shown in Fig. 5(a), by gating the E_γ spectrum shown in Fig. 4(a) with the β-ray energy at $E_\beta \geq 10$ MeV. We note that the 331(2)-keV γ ray was still observed, while the 295(2)-keV peak disappeared. In addition, a minor peak at $E_\gamma = 217(2)$ keV, as seen in Fig. 4(a), is clearly observed in Fig. 5(a). Although the Th decay-chain isotope ^{228}Ac could be a possible BG event, the 217(2)-keV γ ray was observed in neither the BG nor ^{17}N measurements, suggesting that the 217(2)-keV peak as well as 331(2)-keV peak originate from the ^{17}B β decay.

These γ rays were further investigated in order to determine their decay parent nuclei based on (i) the coincidence to β-n emission and (ii) the time evolution of the γ-ray peak counting rates. For determining (i), a γ-ray energy spectrum obtained with the a Ge detector was plotted for β-n-γ triple coincidence events. From the resulting E_γ spectrum shown in Fig. 5(b), no peaks were identified within the given statistics at $E_\gamma = 217(2)$ and 331(2) keV, indicating that these γ rays were not associated with neutron-emission channels in the ^{17}B β decay. As described by point (ii), the time evolution of the photo-peak counting rates was deduced to identify a parent nucleus. A time stamp recorded with E_γ was the time of a β-γ coincidence event measured from the arrival time of a ^{17}B particle, which started at T_{C}, as shown in Fig. 3. Thus, the time evolution in this analysis provides the β-decay lifetime of a parent nucleus feeding the relevant γ emission. The obtained time spectra for 217(2), 295(2), and 331(2) keV are shown in Figs. 6(a), (c), and (d), respectively. Dotted lines shown in the spectra represent the result of a least χ^2 fitting analysis with an exponential function having a known ^{17}B halflife, $t_{1/2}(^{17}$B$)$, plus a constant. The time spectra of 217(2) and 331(2) keV are well reproduced by $t_{1/2}(^{17}$B$)$, unlike the time spectrum of 295(2) keV,

which is rather flat, suggesting a long lifetime of the feeding β decay. This flat spectrum is similar to the 242(1)-keV γ line in Fig. 6(b), which is a BG γ emission line. With regard to the two points described above, we concluded that the 217(2)- and 331(2)-keV γ rays are emitted subsequent to the ^{17}B β decay in the 0n channel, while the 295(2)-keV γ rays is emitted by long-lifetime daughter isotopes produced in the β-decay chain from ^{17}B. The source of the 295(2)-keV γ ray was not identified due to its long lifetime, as compared with the present value of the counting period $T_{\rm C} = 18$ ms.

Finally, an E_γ spectrum obtained from the β-γ-γ triple coincidence measurement was plotted to determine whether the 217(2) and 331(2)-keV γ rays can be assigned to a direct transition to the GS or a cascade transition. The second γ-ray coincidence was detected with the set of thin plastic scintillators and NaI(Tl) detectors mentioned above, wherein the signal from the plastic scintillator was used to remove β-ray events. Figure 5(c) shows an E_γ spectrum obtained in coincidence with the second γ ray at $E_\gamma \leq 400$ keV, measured with the NaI(Tl) detectors. This energy value was selected to investigate the cascade decay below the neutron threshold $S_{\rm n} = 0.729(18)$ MeV. Since no peaks were found at the energy values $E_\gamma = 217(2)$ and 331(2) keV in Fig. 5(c), we concluded that these two γ rays are emitted from the levels $E_{\rm x} = 217(2)$ and 331(2) keV during the transition to the GS in ^{17}C.

3. Other γ lines

Other observed γ lines, whose sources are not clear, are plotted in Fig. 6. The time evolution of the γ lines at $E_\gamma = 743(3)$, 1767(6), 2212(10), 2322(6), and 2379(7) keV, as shown in Figs. 6(e), (l), (n), (o), and (p), respectively, are well reproduced by $t_{1/2}(^{17}$B), indicating that these γ lines were directly fed by the ^{17}B β decay, without the involvement of any daughter isotope β decays. As shown in Fig. 7, the 743(3)-keV γ line was identified as the de-excitation γ line of the $I^\pi = 5/2^+$ state at $E_{\rm x} = 743(2)$ keV $\rightarrow 1/2^+$ GS in ^{15}C, while the γ lines at $E_\gamma = 1767(6)$, 2212(10), 2322(6), and 2379(7) keV were identified as the de-excitation γ lines from the $E_{\rm x} = 1766(10)$, 3986(7), 4088(7), and 4142(7) keV states in ^{16}C, respectively. The γ line at $E_\gamma = 4782(10)$ keV observed in Fig. 4(c) agrees with the γ line of 4780(100) keV $\rightarrow$ GS for ^{15}C. As shown in Fig. 6(q), however, its time evolution is flat, suggesting that the feeding β decay is different from the ^{17}B β(-n) decay. Its source was not identified in this study. In all β-decay channels associated with β-n emission, the time

evolution becomes flat for the given T_C window due to the long lifetimes of the daughter nuclei. The γ lines at $E_\gamma = 1382(5)$ and $1855(8)$, shown in Figs. 6(j) and (m), respectively, correspond to the de-excitation γ lines at 1373.8(3) and 1849.5(3) keV in ^{17}N, which are β-γ decays of the daughter nucleus ^{17}C in the 0n channel of the ^{17}B β decay. Further, in the 2n channel, the γ line observed at 5290(12) keV was identified as the 5298.822(14)-keV γ line in the ^{15}C β-γ decay. Other peaks at $E_\gamma = 770(2)$, 936(2), 1123(3), and 1242(5) keV were also investigated by studying their time evolution, as shown in Figs. 6(f), (g), (h), and (i), respectively; no direct correlation of these peaks with the ^{17}B β decay was observed. They were likely emitted from the decay chain; however, the transitions that caused these peaks could not be identified in this study.

4. *Transition strengths in the 0n channel*

Strengths I_γ of the observed γ lines per ^{17}B β decay were determined using the following equation.

$$I_\gamma = \frac{N_\gamma}{N(^{17}\text{B}) \cdot \epsilon_\gamma \Omega_\gamma \cdot \epsilon_\beta \Omega_\beta \cdot R_\beta} \tag{11}$$

Here, N_γ is the photo peak count, $N(^{17}\text{B})$ are implanted ^{17}B particles, $\epsilon_\gamma \Omega_\gamma$ and $\epsilon_\beta \Omega_\beta$ are, respectively, the overall detection efficiencies of the Ge detector and the β-ray telescopes, including their solid angles, which are evaluated based on the simulation code of GEANT [41]. R_β is the probability that a β decay of a parent nucleus is directly feeding a relevant β-γ-ray emission within the duration T_C. The R_β values were obtained from a simulation based on the following equation

$$R_\beta = \sum_i \int_0^{T_i'} \mathrm{d}t\, f(t; \lambda_1) F(T_i' + t; \lambda_2)(1 - F(T_C; \lambda_2)), \tag{12}$$

$$(T_i' = T_i + T_R)$$

where $f(t; \lambda) = \lambda \exp(-\lambda t)$ is the exponential probability density distribution with a decay constant $\lambda = 1/\tau$, $F(t; \lambda)$ is its cumulative distribution function, λ_1 is the inverse of the meanlife of the ^{17}B β decay, λ_2 is that of the daughter's β-decay constant that directly feeds a relevant γ-ray emission, and T_i is the arrival time of ith ^{17}B particle at which the $T_R + T_C$ gate opens after the first implantation. The probability distribution of T_i is also given by $f(t; \lambda_B)$ with the average ^{17}B beam arrival rate $\lambda_B = 17.3$ pps.

The transition strengths I_γ of the γ line, for which decay schemes were identified, were determined using Eq. (11). The resulting I_γ values, as well as the corresponding values obtained after converting them to I_β and $\log ft$, are listed in Table II. In the derivation of the I_β value associated with the 1767(6)-keV γ line, the contributions from the cascade transitions from $E_\gamma = 2212(10)$, 2322(6), and 2379(7) keV were subtracted. It should be noted that the I_β values for $E_\gamma = 2212(10)$, 2322(6), and 2379(7) keV can include the sum of other β-decay transitions in the 1n channel that are followed by that particular γ ray emission, because these three γ decays could be a part of cascade γ decays from the higher E_x levels.

It is known that in the ^{17}C β decay, β-γ rays are emitted with $E_\gamma = 1373.8(3)$ and 1849.5(3) keV with the transition strengths $I_\gamma^{1374}(^{17}\mathrm{C}) = 24(8)\%$ and and $I_\gamma^{1850}(^{17}\mathrm{C}) = 22(5)\%$, respectively [42]. With the I_γ values obtained from the above analysis for the discussed γ lines and the two mentioned $I_\gamma(^{17}\mathrm{C})$ transition strengths, the total 0n-channel probability $P_{0\mathrm{n}}$ can be derived by using the equation $P_{0\mathrm{n}} = I_\gamma/I_\gamma(^{17}\mathrm{C})$. By taking the weighted average of the resulting probabilities, $P_{0\mathrm{n}}(1382(5) \text{ keV}) = 25(9)\%$ and $P_{0\mathrm{n}}(1855(8) \text{ keV}) = 21(5)\%$, we obtained $P_{0\mathrm{n}} = 25(5)\%$. This probability agrees with the reported $P_{0\mathrm{n}} = 21(2)\%$ [39], within the assigned error bounds.

B. 1n-decay branches

In the one-neutron (1n) decay channel, ^{17}B decays into the levels above the neutron threshold $S_\mathrm{n} = 0.729(18)$ MeV. All of these branches are connected with the GS of ^{16}C. If a transition is connected with an excited state in ^{16}C, the neutron emission is further followed by the de-excitation γ ray emission. The subsequent β decay of ^{16}C, whose halflife is $t_{1/2}(^{16}\mathrm{C}) = 747(8)$ ms [12], is similarly followed by the neutron emission to ^{15}N with $\sim$100% branches in all. This described decay cascade stops at the stable nucleus ^{15}N.

Thus, the 1n-decay channel has been studied through the measurement of β-n [24], in which four excited states of ^{17}C, i.e., $E_\mathrm{x} = 1.18$, 2.25, 2.64, and 3.82 MeV, were identified using a TOF measurement, assuming the direct 1n-decay transition to the ^{16}C GS for all branches. In the present measurement, the Ge and NaI(Tl) detectors were well tuned to detect and thoroughly investigate de-excitation γ rays in ^{16}C through β-n-γ triple coincidence measurements.

1. TOF measurement of β-delayed neutrons

Figure 8 shows the obtained neutron TOF spectra for the emitted neutrons from the ^{17}B β decay; they are measured with (a) high-energy and (b) low-energy neutron detector arrays, and the multiplicity of the neutron is limited to $M_n = 1$. As clearly seen in Fig. 8(a), three peaks can be identified at 64, 81, and 122 ns, which correspond to the neutron kinetic energies $E_n = 3.01$, 1.86, and 0.82 MeV, respectively. Since it is known that in the ^{16}C β decay ($t_{1/2} = 747(8)$ ms), β-n are emitted at $E_n = 0.82(1)$ and 1.70(1) MeV [24], the observed 0.82-MeV peak can be assigned to 0.82(1) MeV. The other two peaks at $E_n = 3.01$ and 1.86 MeV can be assigned to the β-n from the ^{17}B β decay. These two major peaks were also observed at almost the same energies $E_n = 2.91(5)$ and 1.80(2) in Ref. [24].

The obtained neutron TOF spectrum shown in Fig. 8(a) was analyzed using the response function (described later in the text) of the neutron detector array. This response function was determined so as to reproduce the well studied β-n from the ^{17}N β decay [34]. In the present analysis, the following four factors were taken into account: (a) the level width of the initial state, (b) uncertainty in the flight path of the neutrons due to the counter misalignment and a finite beam-spot size, (c) the long low-energy tail due to the scattering of emitted neutrons from materials around the Pt stopper, and (d) uncertainty in the time resolution, such as the intrinsic time resolution of the β and neutron detectors. In order to account for factor (a), the response function essentially assumes a Lorentzian function $H(t)$, and it includes the additional term $f(t)$ to account for factor (c), where $f(t)$ is empirically determined. The response function $\mathcal{F}(t)$ is then obtained as a Gaussian convolution of $H(t)+f(t)$ to account for factors (b) and (d). Thus, the function $\mathcal{F}(t)$ uses three parameters, the amplitude of peaks, the neutron kinetic energy E_n, and the level width Γ. The detailed description of $\mathcal{F}(t)$ is given in Ref. [28].

Next, peak-decomposition was conducted through the least χ^2-fitting analysis with the obtained $\mathcal{F}(t)$ function. In this analysis, the following three types of BGs were taken into account: (i) neutrons emitted in the multi-neutron emission channel initiated by the ^{17}B β decay, which was assumed to have a Gaussian shape with a wide width at the position $\sim$100 ns, empirically determined from a TOF spectrum of neutrons, measured with the neutron multiplicity $M \geq 2$; (ii) scattered β rays expressed by a spectral curve monotonically decreasing with t; and (iii) a constant BG. The β-n emitted from the β decay of ^{16}C, for

$E_n = 0.82(1)$ and $1.70(1)$ MeV, were also considered, and the reported relative intensities were fixed in this case. The result of the fitting analysis is shown in Fig. 8(a) using dashed curves. Other than the two major peaks, which were determined to be at $E_n = 3.01(1)$ and $1.86(1)$, the existence of minor peaks corresponding to neutron kinetic energies $E_n = 5.04(2)$, $3.81(1)$, and $1.46(1)$ MeV was suggested. Ref. [24] has reported two minor transitions at $E_n = 1.43(2)$ and $0.42(1)$ MeV. The first E_n value listed agrees with the present $E_n = 1.46(1)$ peak, with only a small difference, although no peak corresponding to the second value was visible in the spectrum. We also investigated neutrons at a lower E_n with the low-energy neutron array. However, in the obtained spectrum shown in Fig. 8(b), no further peaks were identified at any E_n down to 0.01 MeV.

2. *Neutron-decay branches to excited states in* ^{16}C

In order to construct the decay scheme, it is necessary to investigate connected states in ^{16}C after neutron emission. Here, we first studied a γ-ray energy spectrum obtained in a β-n-γ triple-coincidence measurement. As shown in Figs. 9(a) and (b), the de-excitation γ rays from the first exited state in ^{16}C at $E_x = 1766(10)$ keV to the GS were clearly identified as a peak in the E_γ spectrum measured using both the NaI(Tl) and Ge detectors. Another peak was also observed at $E_\gamma = 743(2)$ keV, which corresponds to the de-excitation γ rays from the ^{15}C excited state at $E_x = 740.0(15)$ keV to its GS following the two-neutron emission in the 2n channel of the ^{17}B β decay. To confirm the initiating β decay feeding the two corresponding E_γ emissions, the time evolution of their counting rates were investigated as in the 0n-channel analysis. Both the consequently obtained time spectra, shown in Figs. 6(e) and (l), were well reproduced by $t_{1/2}(^{17}$B$)$, which shows that these γ emissions were directly fed by the ^{17}B β decay. Further, two small peaks are observed in Fig. 4(b) at $E_\gamma = 2322(6)$ and $2379(7)$, which agrees with the de-excitation γ lines $2322(6)$ and $2379(7)$ keV from the $3^{(+)}$ state at $E_x = 4088(7)$ keV and the 4^+ state at $E_x = 4142(7)$ keV on ^{16}C, respectively. The time-evolution analysis described above was also performed for these two E_γ lines, and the results are shown in Figs. 6(o) and (p), respectively. Although the statistics are not sufficient, they are reproduced by $t_{1/2}(^{17}$B$)$, suggesting that the ^{17}B β decay directly feeds these two γ emissions through β-n emissions. Although peaks should appear at $E_\gamma = 2322(6)$ and $2379(7)$ in the gated E_γ spectrum shown in Fig. 9, they are not observed due to the

limited statistics.

In the next step, β-n components connected to the $E_{\mathrm{x}} = 1766(10)$ keV state in ^{17}C were investigated. Figure 10 shows a neutron TOF spectrum measured under the β-n-γ coincidence condition, and in the measurement E_γ energies were set as $E_\gamma \simeq$ (a) 1767 keV and (b) 2400 keV. To enable clear comparison, the normalized TOF spectrum without the E_γ window (i.e., the spectrum shown in Fig. 8(a)) is also drawn using gray lines. In both the spectra, two major peaks at $E_{\mathrm{n}} = 3.01(1)$ and 1.86(1) MeV still appear. However, this does not imply that the two peaks are connected to the 1767(6)-keV γ line. The peaks are caused by accidental coincidences owing to the following two reasons. First, The TOF spectrum obtained for $E_\gamma = 2400$ keV, at which no Compton scattering from the $E_\gamma = 1767(6)$ keV γ rays can interfere and no other photo peaks are observed, is analogous to the spectrum in the ungated case, as shown in Fig. 10(b). In addition, the obtained counting rates of the two major peaks are ~20 times smaller than those expected on the basis of the spectrum shown in Fig. 8(a) and the given NaI(Tl) efficiency. If we closely examine Fig. 10(a), however, a peak can be observed at ~95 ns, which is emphasized by the $E_\gamma = 1767(6)$ keV gate. This peak energy, $E_{\mathrm{n}} = 1.51(6)$ MeV, agrees with the $E_{\mathrm{n}} = 1.46(1)$ MeV obtained in the described peak decomposition analysis of the ungated E_{n} spectrum. In addition, the transition strength $I_\beta = 1.7(2)\%$, evaluated using the 1.51-MeV peak count based on Eq. (14), which accounts for the NaI(Tl) efficiency, agrees with the value $I_\beta = 1.5(2)\%$ for the 1.46-MeV peak determined as described in Sec. IIIB4. It is then natural to conclude that both the peaks are identical. No peaks are observed at $E_{\mathrm{n}} = 5.04(2)$ and 3.81(1) MeV in Fig. 10(a), although peaks with statistics comparable to the $E_{\mathrm{n}} = 1.46(1)$ peak should be observed if they are also connected to the $E_{\mathrm{x}} = 1766(10)$ keV state.

3. Neutron-decay branches to the ^{16}C ground state

Because it was shown that only the 1.46(1)-MeV peak was connected to the 1767(6)-keV γ line, the two major peaks at $E_{\mathrm{n}} = 3.01(1)$ and 1.86(1) MeV, as well as the minor peaks at $E_{\mathrm{n}} = 5.0$ and 3.8 MeV, were assigned to the direct transition to the ^{16}C GS. As described in the following text, this assignment was verified with the $E_{\mathrm{n}} = 1.86(1)$ MeV peak having the highest statistics, through the measurement of the end-point energy E_β^{max}

of the β decay associated with this E_n peak. Figure 11(b) shows a β-ray energy spectrum of the ^{17}B β decay obtained with the combination of the NaI(Tl) and plastic scintillators in the β-n measurement by gating at $E_n = 1.86(1)$ MeV. The spectrum is expressed in the form of the Kurie plot $\sqrt{N(E)/pEF(Z,E)}$, where E and p are of the total energy and momentum of the β particle, $N(E)$ is the observed β-ray yield at E, $F(Z,E)$ is the Fermi function, and Z is the atomic number of the parent nucleus. The obtained β-ray energy spectrum was analyzed using a GEANT [41] simulation, in which an arrowed β-decay transition was assumed by taking into account its $\log ft$ value 4.8(1), determined in the present work, as explained later. The obtained end-point energy $E_\beta^{\max} = 19.7(1)$ MeV agrees well with the 19.9(1) MeV value for the transition to the ^{16}C GS calculated using the Q_β of ^{17}B and the neutron energy $E_n = 1.86(1)$ MeV, while it differs from $E_\beta^{\max} = 18.1(1)$ MeV when the β-n emission is connected to the 1767(6) keV γ emission line. The accuracy of the analysis was evaluated using the ^{15}B β decay measured in the present work. It is known that in the ^{15}B β decay, the transition to $E_x = 3.10$ MeV, which has the highest transition strength in the β decay, is followed by the $E_n = 1.76$ MeV β-n emission [22, 28]. Thus, a Kurie plot was also obtained for this transition using the same experimental apparatus. As shown in Fig. 11(a), the end-point energy $E_\beta^{\max} = 15.5(1)$ MeV obtained through the same procedure again agrees with the calculated value $E_\beta^{\max} = 16.0(1)$ MeV, with only a slight difference in values. Due to the limited statistics, this analysis cannot be carried out for the remaining minor peaks at $E_n = 5.0(3)$ and 3.8(1) MeV.

4. Transition strengths in the 1n channel

As mentioned above, the ^{17}B β decay in the 1n channel is 100%, followed by the successive β-n emission in the β decay of the daughter nucleus of ^{16}C. Because in the ^{16}C β decay, the strength of the transition feeding the β-n emission at $E_n = 0.82(1)$ is known to be $I_\beta = 84.4(17)\%$, the total 1n decay strength P_{1n} of the ^{17}B β decay can be determined by

$$P_{1n} = \frac{N_n}{N(^{17}\text{B}) \cdot I_\beta \cdot \epsilon_n \Omega_n \cdot \epsilon_\beta \Omega_\beta \cdot R_\beta}, \tag{13}$$

where N_n is the count of the 0.82(1)-MeV peak obtained in the described χ^2-fitting analysis and ϵ_n and Ω_n are the efficiency and the solid angle of the neutron counter array for the 0.82(1)-MeV neutron. The values of ϵ_n were evaluated based on Ref. [35], using experimental

ϵ_n data obtained from the measurements separately conducted with ^{17}N and ^{15}B beams, as described in Sec. II B. Here, the ϵ_n of the β-n at $E_n = 1.17$ MeV in the β decay of ^{17}N, which is close to 0.82(1) MeV, was determined with an accuracy of $\Delta\epsilon_n = 9.4\%$. The same $\Delta\epsilon_n$ value was therefore adopted in the evaluation of ϵ_n for the 0.82(1)-MeV neutron as a systematic error. We thus obtained $P_{1n} = 67(7)\%$, which agrees with the reported value $P_{1n} = 63(1)\%$ [39], within the assigned error bounds.

However, for the other E_n energies of observed β-n, the accuracies of the obtained ϵ_n reference data were not sufficiently high. Therefore, the 1n transition strengths were determined by solving for the normalization factor α in the following equation

$$P_{1n} = \alpha \left(\sum_i I'_\beta(i) - I'_\beta(1.46 \ \text{MeV}) \right) + 9.4\%, \tag{14}$$

where $I'_\beta(i)$ is the relative transition strength obtained with a relative ϵ_n value for each transition i and 9.4% is the sum of the strengths of the 1n transitions that are finally followed by $E_\gamma = 1767(6)$ keV γ ray emissions, which were not included in the left-hand side in Eq. (14), with the exception of $I'_\beta(1.46 \ \text{MeV})$. The resultant I_β values calculated using $\alpha I'_\beta$, as well as the values obtained by converting them to $\log ft$ and $B(\text{GT})$, are summarized in Table III.

C.   2n-decay and the higher-multiplicity channels

The ^{17}B β decay in the 2n-decay channel feeds states in ^{15}C through the β-2n emission. All 2n-decay branches are then followed by the β decay of ^{15}C ($t_{1/2} = 2.449(5)$ s [43]), where the $E_\gamma = 5290(12)$ keV γ ray is expected be emitted from the $I^\pi = 1/2^+$ excited state at $E_x = 5298.822(14)$ keV in ^{15}N, with the branching ratio $I_\beta^{5299}(^{15}\text{C}) = 63.2(8)\%$ [44]. The corresponding peak was observed at $E_\gamma = 5290(12)$ keV in the obtained Ge spectrum, as shown in Fig. 4(c), for which the deduced transition strength $I_\gamma(^{17}\text{B}) = 7.5(11)\%$ is listed in Table II. The total 2n-decay probability, P_{2n}, can then be determined as $P_{2n} = I_\gamma^{5290(12)}(^{17}\text{B})/I_\beta^{5299}(^{15}\text{C}) = 12(2)\%$. It should be noted that this P_{2n} value agrees well with the value $P_{2n} = 11(7)\%$ reported in Ref. [39], within the assigned error bounds.

In the 2n channel, the γ ray observed at $E_\gamma = 743(2)$ keV in Fig. 4(a) can be assigned to the de-excitation γ ray from the $I^\pi = 5/2^+$ first excited state at $E_x = 740.0(15)$ keV [44] to the $I^\pi = 1/2^+$ GS of ^{15}C. This assignment was confirmed by observing that the time

20

evolution of the photo-peak counts, shown in Fig. 6(e), can be well reproduced by $t_{1/2}(^{17}\text{B})$. From the measured peak count, the sum of the strengths of the ^{17}B β-decay transitions connected to the $E_\text{x} = 740.0(15)$ keV state of ^{15}C was determined to be $I_\beta = 2.6(2)\%$, as listed in Table II. Since no γ lines of ^{15}C, other than the one at 743(2) keV, were identified in the E_γ spectrum, we concluded that the 740.0(15)-keV state is directly connected to the two-neutron emission and that the GS of ^{15}C is directly fed by the strength $P_\text{2n} - I_\beta = 9.4(3)\%$. In order to construct the decay scheme of the 2n-decay channel, it is necessary to identify the sum energy of the two emitted neutrons. However, the obtained statistics provided no clear evidence of the 2n decay.

With respect to the 3n(4n)-decay branch, the β-n emission from ^{17}B feeds states in $^{14}\text{C}(^{13}\text{C})$, for which the total transition probability is reported to be $P_\text{3n} = 3.5(7)\%$ ($P_\text{4n} = 0.4(3)\%$) [39]. Because the halflife of ^{14}C is $t_{1/2} = 5730$ y and ^{13}C is stable, the β-decay cascade from ^{17}B is almost stopped at the GSs. In the measurement, clear peaks were not found in the sum-energy spectra of neutrons with multiplicity $M_\text{n} = 3$ or 4 with the present statistics. Furthre, no γ-ray peaks were found at the E_γ energies associated with the de-excitation γ rays in ^{13}C and ^{14}C. Thus, both P_3n and P_2n were not determined in the present work.

D. Spin-parity assignment

After obtaining the peak counts of the β-n TOF spectra in the peak-decomposition analysis, $A_\beta P$ values of the transition to $E_\text{x} = 2.71(2)$, 3.93(2), and 4.05(2) MeV, for which two unassigned peaks were removed, were determined based on Eq. (4), and the values are listed in Table III. In order to determine I^π values, the least P-variance method described in Sec. II D was applied to the obtained $A_\beta P$ values. For all possible $3^3 = 27$ combinations of I^π, χ_ν^2, given by Eq. (9), were calculated together with the corresponding mean spin polarization $\bar{P}$, defined in Eq. (7). The resulting χ_ν^2 values are plotted as a function of $\bar{P}$ in Fig. 12. The obtained χ_ν^2 values can be divided into three groups, as indicated by the dotted ellipses in Fig. 12: $\bar{P} \simeq -2.5$, -1.5, and $+2.4\%$. This classification is based on the I_f^π value of the 2.71(2)-MeV state owing to its highest statistics.

We first note that a negative spin polarization is expected for the ^{17}B beam produced in the present experiment, based on the systematics observed with similar beam energies,

targets, and projectile-ejectile combinations [9, 26, 27, 31, 45–49], for which the reaction proceeds through a far-side trajectory owing to the nuclear attractive force dominating the Coulomb repulsive force. Actually, the negative spin polarization of ^{15}B, $\bar{P} = -2.81(42)\%$, was observed with the same beam energies, targets, and projectile [28]. Thus, the possibility of assigning $5/2^-$ to the 2.71(2)-MeV state can be eliminated owing to its positive polarization $\bar{P} \simeq +2.4$. Among the remaining two I^π values, $1/2^-$ and $3/2^-$, the former can be assigned using the obtained minimum χ^2_ν analysis, although the possibility that $3/2^-$ can be assigned is not possible to completely ignore.

After we assigned $1/2^-$ to the 2.71(2)-MeV state, the I^π combinations could be further divided into two groups: (i) $1/2^-$ and (ii) $3/2^-$ or $5/2^-$ assignments for the 3.93(2)-MeV state. The χ^2_ν values of the first group are in the range of $0.49 \sim 0.51$, whereas the second group has a smaller $\chi^2_\nu = 0.12 \sim 0.26$. We thus assigned $(3, 5)/2^-$ to the 3.93(2)-MeV state. However, no further I^π selection was performed, because the differences among the six combinations in the second group were extremely small. The I^π assignment completed in this analysis is listed in Table III, together with the asymmetry parameters calculated from the expected polarization $\bar{P} = 1.5(8)$ and given by the minimum χ^2_ν set.

IV. DISCUSSION

A. Further investigation for I^π assignments

The obtained level structure of ^{17}C was further investigated for comparison with the β decays of ^{13}B and ^{15}B. The several negative-parity states in ^{13}C (^{15}C), connected with the β decay of ^{13}B (^{15}B), are illustrated in Fig. 14, where relative $B(\text{GT})$ strengths calculated from the reported $\log ft$ values [44] are indicated by the line thickness, assuming that Fermi transition strengths are negligibly small owing to the large difference between their $E_\beta{}^{\text{max}}$ energies and Q_β values. In the β decay of ^{13}B, the transition strength is concentrated at the β-decay branch leading to the $1/2_1^-$ GS of ^{13}C, whose branching ratio is 92.1%. Including the second strongest branch with the strength 7.6%, leading to the $3/2_1^-$ excited state at $E_{\text{x}} = 3684.507(19)$ keV, the sum of the ^{13}B β-decay transitions exhausts $\sim 100\%$ of the total transition strength. Because the main GS configuration of ^{13}B can be described by $|^{13}\text{B}_{\text{GS}}\rangle^{3/2^-} = |(\pi p_{3/2})_{-1} \otimes (\nu p_{3/2})_4^{0^+} (\nu p_{1/2})_2^{0^+}\rangle^{3/2^-}$, given the well-established neutron magic

22

number $N = 8$, the transition to the $1/2_1^-$ GS can be described by the single-particle GT transition $\nu p_{1/2} \to \pi p_{3/2}$, under the reasonable assumption of a configuration $|^{13}\mathrm{C_{GS}}\rangle^{1/2^-} = |(\pi p_{3/2})_4^{0^+} \otimes (\nu p_{3/2})_4^{0^+} (\nu p_{1/2})_1\rangle^{1/2^-}$ to the $1/2_1^-$ state. Then, the concentration of the transition strength to the $1/2_1^-$ state can be understood taking this pure single $\nu p_{1/2}$-particle state to the $1/2_1^-$ state, because the $\nu p_{1/2} \to \pi p_{3/2}$ GT transition can only populate this configuration from the ^{13}B GS. A similar observation applies to the ^{15}B β decay, in which the lowest negative-parity state at $E_\mathrm{x} = 3.103$ MeV [44] in ^{15}C, which has been assigned to $I^\pi = 1/2^-$ [22, 28], is fed through the strongest GT transition. Assuming a weak coupling of the ^{13}B GS with the two valence neutrons in the sd orbit, the ^{15}B GS can be written as $|^{15}\mathrm{B_{GS}}\rangle^{3/2^-} = |^{13}\mathrm{B_{GS}}\rangle^{3/2^-} \otimes |(\nu sd)_2\rangle^{0^+}$. Then, the observed analogous characteristics of the GT transitions in the β decays of ^{13}B and ^{15}B can be understood, provided a major contribution of the GT transition from ^{15}B to the lowest $1/2^-$ state in ^{15}C is largely governed by the $\nu p_{1/2} \to \pi p_{3/2}$ transition in the ^{13}B GS, where the two neutrons are kept in the sd orbit to couple to form $I^\pi = 0^+$. For detailed discussions, such as those on the inversion of the $3/2_1^-$ and $5/2_1^-$ states in ^{15}C, effects of the p-sd cross-shell interactions need to be taken into account. The same rule can be applied to the ^{17}B β decay, because the main configuration of the ^{17}B GS should be given by $|^{17}\mathrm{B_{GS}}\rangle^{3/2^-} = |^{13}\mathrm{B_{GS}}\rangle^{3/2^-} \otimes |(\nu sd)_4\rangle^{0^+}$. Then, the strongest GT transition can be characterized by $\nu p_{1/2} \to \pi p_{3/2}$ in the ^{13}B GS, and the final state is described by $I^\pi = 1/2^-$, which would be the lowest negative-parity state. Factually, among the observed β-decay transitions from ^{17}B, the strongest transition $I_\beta = 33(4)\%$ is the branch to the $E_\mathrm{x} = 2.71(2)$ MeV state in ^{17}C, to which $I^\pi = 1/2^-$ has been assigned in the present χ_ν^2 analysis. The relative $B(\mathrm{GT})$ strengths of the ^{17}B β decay are also shown in Fig. 14 in a similar manner as for ^{13}C and ^{15}C.

The decay branch to the $3/2_1^-$ state is the second strongest transition in both the β decays of ^{13}B and ^{15}B, although the ordering of $3/2_1^-$ and $5/2_1^-$ differs for ^{13}C and ^{15}C due to the appearance of the p-sd cross-shell interactions in ^{15}C. These transitions are considered to be related to the single particle GT transition $\nu p_{3/2} \to \pi p_{3/2}$, which results in the $\nu p_{3/2}$-hole configurations in the daughter nuclei ^{13}C and ^{15}C. Similar to the above $1/2_1^-$ case, the $\nu p_{3/2} \to \pi p_{3/2}$ GT transition can uniquely populate the single $\nu p_{3/2}$-hole state, suggesting its large transition strength. The same single-particle GT transition can also occur in the ^{17}B β decay. The gap energy between the $\nu p_{3/2}$- and $\nu p_{1/2}$-hole states should be comparable in both ^{15}C and ^{17}C, provided the spin-orbit splitting remains relatively unchanged. From

this viewpoint, $I^\pi = 3/2^-$ can be assigned to the 3.93(2)-MeV state in ^{17}C, because the energy difference $\Delta E = 1.22$ MeV between the 3.93(2)-MeV state and $1/2^-$ 2.71(2)-MeV state in ^{17}C is comparable to $\Delta E = 1.55$ MeV, which is the difference between the $1/2_1^-$ and $3/2_1^-$ states in ^{15}C, and also because the second strongest B(GT) value was obtained for the transition to the 3.93(2)-MeV state. It should be noted that this I^π assignment agrees with the $I^\pi = (3, 5)/2^-$ assignment in the present χ_ν^2 analysis.

We may assign $5/2^-$ to the 4.05(2)-MeV state, which is a neighboring partner state to the $3/2_1^-$ 3.93(2)-MeV state, by taking into account the similarity of the level structure in this case to that of ^{15}C, although we cannot disregard the fact that there are three possible candidates $I^\pi = (1, 3, 5)/2^-$ in the χ_ν^2 analysis. The obtained $\log ft = 6.0(1)$ value for the transition to the 4.05(2)-MeV state is not sufficiently small to be definitely assigned to the GT transition. However, $\log ft$ values to the corresponding $5/2_1^-$ states at 7.547 and 4.220 MeV in ^{13}C and ^{15}C are also as large as $\log ft = 5.33(10)$ [44] and 5.09(9) [22], respectively, indicating the similarity among their transitions strengths. As investigated in the above, the GT transition $\nu p_{3/2}(\nu p_{1/2}) \to \pi p_{3/2}$ uniquely populate the $1/2_1^-(3/2_1^-)$ state having single $\nu p_{1/2}$-particle ($\nu p_{3/2}$-hole) state properties, which causes the concentration of transition strengths. However, the $5/2_1^-$ state cannot be formed by an unpaired particle or hole in the p-sd shell unlike the $1/2_1^-$ and $3/2_1^-$ states. It should be a mixed configuration such as $|^{17}\text{C}\rangle^{5/2^-} = |((\pi p_{1/2})_1(\pi p_{3/2})_{-1})^{1^+,\,2^+} \otimes (\nu p_{3/2})_{-1}(\nu sd)_4^{0^+}\rangle^{5/2^-}$, which prevents the concentration of the transition strength. Moreover, the GT transition $\nu p_{3/2}(\nu p_{1/2}) \to \pi p_{1/2}$, which can populate these configurations, can also populate the states up to $I^\pi = 7/2^-(5/2^-)$, further fragments the transition strength. Thus, the $5/2^-$ assignment to the 4.05(2)-MeV state seems reasonable, although further experimental observations are necessary for a definite assignment.

Including the above mentioned I^π assignment, results obtained in the present work for the ^{17}B β decay are shown in Fig. 13 as the decay scheme.

B. Comparison with shell-model calculations

In Fig. 14, the data of the excited states of ^{17}C observed in the present study are compared with the results of shell-model calculations [50] with two different sets of effective interactions, PSDWBT [51] and PSDMK [52], denoted by WBT and MK, respectively.

With respect to the low-lying positive-parity states, the GS has been experimentally assigned to $I^\pi = 3/2^+$ [3–9], and the 210-keV and 331-keV states have been assigned to $1/2^+$ and $5/2^+$ [17–19]. Here, we assumed that the excited state at $E_x \sim 210$ keV and the observed 217(2)-keV state are identical. The shell-model calculations predict the existence of three positive-parity states, $I^\pi = 3/2^+$, $1/2^+$, and $5/2^+$, below the neutron separation energy $S_n = 0.729(18)$ MeV. However, their ordering changes, depending on the choice of effective interactions. For the I^π value of the GS, the MK interaction predicts the $3/2^+$ correctly, whereas the WBT interaction predicts $5/2^+$. The experimental and theoretical positive-parity states in ^{17}C are indicated by dashed lines in Fig. 14. We note that the experimentally determined ordering of $1/2^+$ and $5/2^+$ is inverted both in the MK and WBT calculations.

Next, the observed negative-parity states were compared. As expected from the above comparison for positive-parity states, the $1/2^-$ state is predicted as the lowest negative-parity state in ^{17}C according to both the WBT and MK interactions, which thus supports the assignment of $1/2^-$ to the $E_x = 2.71(2)$ MeV state. The E_x energy for this state, predicted using the MK interaction, agrees well with the observation, while it is ~ 1 MeV lower when determined using the WBT interaction. For the next two states at 3.93(2) and 4.05(2) MeV, $I^\pi = 3/2^-$ and $(5/2^-)$ were respectively assigned herein. The energy gap of their centroid, whose displacement is only 110 keV from the GS, is 6.0 MeV. Such a pair of neighboring states are also predicted using both the MK and WBT interactions. The MK interaction predicts the $5/2^-$ and $3/2^-$ states at $E_x = 4.62$ and 4.69 MeV, respectively, for which the centroid is ~ 0.7 MeV higher than in the experimental observation. In contrast, the ordering is inverted in the WBT calculation, where the $3/2^-$ and $5/2^-$ states are predicted at $E_x = 3.09$ and 3.26 MeV, respectively. In this case, the centroid is lower by ~ 0.8 MeV in the direction opposite to that observed in the MK interaction. If we calculate E_x for them using the $3/2_1^+$ state instead of the predicted $5/2_1^+$ GS, the difference is found to be ~ 0.9 MeV. Thus, the WBT interaction based calculation systematically predicts ~ 1 MeV lower E_x energies for all the low-lying negative-parity states.

In the light mass region, the phenomena of reduction in the single particle energy of the $s_{1/2}$ state are known to occur for $N = 7$ [1] and $N = 9$ [2] nuclei. However, the ~ 1 MeV discrepancy due to the tendency of the energies of negative-parity states in ^{17}C to be calculated as lower with the WBT interaction cannot be corrected by lowering the $s_{1/2}$

single particle energy. The ^{17}C energy levels calculated by reducing the original $s_{1/2}$ single particle energy $\epsilon_{\text{s. p.}}(s_{1/2})$ to $\epsilon_{\text{s. p.}}(s_{1/2}) - 1$ MeV are also shown in Fig. 14. This modification changes the energies E_{x} of the positive-parity states, and in particular, the ordering of the low-lying states, while it does not affect the energies E_{x} of the negative-parity states. In fact, the energy displacement from the $3/2_1^+$ state is further lowered, and hence, the discrepancy from the experimental observation is rather exacerbated.

A further investigation was performed with the WBT interaction. In this study, the WBT calculation was performed, with the $|V_{01}|$ values reduced by 30%, for the sd neutrons, and herein, $|V_{01}|$ denotes a diagonal matrix element of a two-body effective interaction in a channel with angular momentum $I = 0$ and isospin $T = 1$ for particles within the sd orbits. The diminished pairing energy is attributed to the following three reasons. First, systematic over-binding occurs for the even mass-number C isotopes ^{16}C, ^{18}C, and ^{20}C with the WBP interaction [51], as reported in the study of binding energies for the neutron-rich C isotopes [11]. Second, the weakening of the coupling between excess neutrons and the core in nuclei away from the stability line causes pairing energies to be modified. A significant amount of theoretical V_{01} values of the two neutrons in the sd shell are originated from the renormalization of the two-body interaction due to the polarization of the core [53]. Finally, it was shown in the study of the GS magnetic-moment measurement of ^{17}B [31] that the use of the pairing energy $|V_{01}|$ reduced by 30% improves agreements of the experimental and theoretical magnetic moments as well as low-lying state energies of neighboring neutron-rich nuclei. In the state structure calculated with the $0.7|V_{01}|$ values, shown in Fig. 14, the energy gap between the GS and the $1/2_1^-$ state becomes as wide as in the experimental observation. Furthermore, the GS described by $I^\pi = 3/2^+$ was correctly reproduced. The ordering of the other low-lying positive-parity states $1/2_1^+$ and $5/2_1^+$ is, however, inverted from the experimental observation in the calculations with both WBT $(0.7|V_{01}|)$ and MK interactions.

V. SUMMARY

By virtue of the large Q_β window, excited states in ^{17}C were effectively investigated through the measurement of β-n and γ rays emitted in the β decay of ^{17}B. In the measurement, three negative-parity states and two inconclusive states, were identified above the

neutron threshold energy in the 1n channel of the ^{17}B β decay. Further, two positive-parity states below the threshold were also observed. For the transitions, experimental I_β values were determined. We note that in the 1n-channel, the 1767(6)-keV γ ray from the first excited state of ^{16}C was observed in coincidence with the emitted β-n, which changes the reported β-decay scheme of ^{17}B and level structure of ^{17}C. Apart from the 1767(6)-keV lines, several de-excitation γ lines connected after the β-n emission were identified. In the present work, the β-NMR technique was combined with the β-delayed particle measurements using a fragmentation-induced spin-polarized ^{17}B beam. This new scheme allowed us to determine the spin parity of β-decay feeding excited states based on the difference in the β-decay asymmetry parameter, which took three discrete values depending on the final state spin for a common initial spin, if the states are connected through the GT transition. As a result, $I^\pi = 1/2^-$, $3/2^-$, and $(5/2^-)$ have been assigned to the observed states at $E_x = 2.71(2)$, $3.93(2)$, and $4.05(2)$ MeV in ^{17}C, respectively. The observed gap energy between low-lying positive and negative-parity states is 1$\sim$2 MeV larger than that predicted by the shell-model calculation with the WBT interaction. This discrepancy can be reduced by assuming that the pairing energy for neutrons in the sd shell of a neutron-rich nucleus diminishes by about 30%, although it cannot be resolved by reducing the $s_{1/2}$ single-particle energy.

Acknowledgments

---

[1] L. Talmi and L. Una, Phys. Rev. Lett. **4**, 469 (1960).

[2] T. Suzuki and T. Otsuka, Phys. Rev. C **50**, R555 (1994).

[3] T. Baumann, M.J.G. Borge, H. Geissel, H. Lenske, K. Markenroth, W. Schwab, M.H. Smedberg, T. Aumann, L. Axelsson, U. Bergmann, D. Cortina-Gil, L. Fraile, M. Hellstrom, M. Ivanov, N. Iwasa, R. Janik, B. Jonson, G. Munzenberg, F. Nickel, T. Nilsson, A. Ozawa, A. Richter, K. Riisager, C. Scheidenberger, G. Schrieder, H. Simon, B. Sitar, P. Strmen,

K. Summerer, T. Suzuki, M. Winkler, H. Wollnik, M.V. Zhukov, Phys. Lett. **B439B**, 256 (1998).

[4] D. Bazin, W. Benenson, B.A. Brown, J. Brown, B. Davids, M. Fauerbach, P.G. Hansen, P. Mantica, D.J. Morrissey, C.F. Powell, B.M. Sherrill, and M. Steiner, Phys. Rev. C **57**, 2156 (1998).

[5] E. Sauvan, F. Carstoiu, N.A. Orr, J.C. Angelique, W.N. Catford, N.M. Clarke, M. Mac Cormick, N. Curtis, M. Freer, S. Grevy, C.Le Brun, M. Lewitowicz, E. Liegard, F.M. Marques, P. Roussel-Chomaz, M.G. Saint Laurent, M. Shawcross, J.S. Winfield, Phys. Lett. **B491**, 1 (2000).

[6] V. Maddalena, T. Aumann, D. Bazin, B.A. Brown, J.A. Caggiano, B. Davids, T. Glasmacher, P.G. Hansen, R.W. Ibbotson, A. Navin, B.V. Pritychenko, H. Scheit, B.M. Sherrill, M. Steiner, J.A. Tostevin, and J. Yurkon, Phys. Rev. C **63**, 024613 (2001).

[7] Y. Satou, T. Nakamura, N. Fukuda, T. Sugimoto, Y. Kondo, N. Matsui, Y. Hashimoto, T. Nakabayashi, T. Okumura, M. Shinohara, T. Motobayashi, Y. Yanagisawa, N. Aoi, S. Takeuchi, T. Gomi, Y. Togano, S. Kawai, H. Sakurai, H.J. Ong, T.K. Onishi, S. Shimoura, M. Tamaki, T. Kobayashi, H. Otsu, Y. Matsuda, N. Endo, M. Kitayama, M. Ishihara, Phys. Lett. **B660**, 320 (2008).

[8] K.W. Scheller, J. Gorres, S. Vouzoukas, M. Wiescher, B. Pfeiffer, K.-L. Kratz, D.J. Morrissey, B.M. Sherrill, M. Steiner, M. Hellstrom, J.A. Winger, Nucl. Phys. **A582**, 109 (1995).

[9] H. Ogawa, K. Asahi, H. Ueno, K. Sakai, H. Miyoshi, D. Kameda, T. Suzuki, H. Izumi, N. Imai, Y.X. Watanabe, K. Yoneda, N. Fukuda, H. Watanabe, A. Yoshimi, W. Sato, N. Aoi, M. Nagakura, T. Suga, K. Yogo, A. Goto, T. Honda, Y. Kobayashi, W.-D. Schmidt-Ott, G. Neyens, S. Teughels, A. Yoshida, T. Kubo, M. Ishihara, Eur. Phys. J. A **13**, 81 (2002).

[10] T. Nakamura, N. Fukuda, T. Kobayashi, N. Aoi, H. Iwasaki, T. Kubo, A. Mengoni, M. Notani, H. Otsu, H. Sakurai, S. Shimoura, T. Teranishi, Y.X. Watanabe, K. Yoneda, M. Ishihara, Phys. Rev. Lett. **83**, 1112 (1999).

[11] D. Bazin, B.A. Brown, J. Brown, M. Fauerbach, M. Hellstrom, S.E. Hirzebruch, J.H. Kelley, R.A. Kryger, D.J. Morrissey, R. Pfaff, C.F. Powell, B.M. Sherrill, M. Thoennessen, Phy. Rev. Lett. **74**, 3569 (1995).

[12] G. Audi, O. Bersillon, J. Blachot, A.H. Wapstra, Nucl. Phys. **A624**, 1 (1997).

[13] J.A. Nolen, T.S. Bhatia, H. Hafner, P. Doll, C.A. Wiedner, G.J. Wagner, Phys Lett. **B71**,

314 (1977).

[14] L.K. Fifield, J.L. Durell, M.A.C. Hotchkis, J.R. Leigh, T.R. Ophel, D.C. Weisser, Nucl. Phys. **A385**, 505 (1982).

[15] R. Kanungo, Z. Elekes, H. Baba, Zs. Dombrádi, Zs. Fülöp, J. Gibelin, Á. Horváth, Y. Ichikawa, E. Ideguchi, N. Iwasa, H. Iwasaki, S. Kawai, Y. Kondo, T. Motobayashi, M. Notani, T. Ohnishi, A. Ozawa, H. Sakurai, S. Shimoura, E. Takeshit, S. Takeuchi, I. Tanihata, Y. Togano, C. Wu, Y. Yamaguchi, Y. Yanagisaw, A. Yoshida, K. Yoshida, Nucl. Phys. **A757**, 315 (2005).

[16] M. Stanoiu , F. Azaiez, F. Becker, M. Belleguic, C. Borcea, C. Bourgeois, B.A. Brown, Z. Dlouhy, Z. Dombradi, Z. Fulop, H. Grawe, S. Grevy, F. Ibrahim, A. Kerek, A. Krasznahorkay, M. Lewitowicz, S. Lukyanov, H. van der Marel, P. Mayet, J. Mrazek, S. Mandal, D. Guillemaud-Mueller, F. Negoita, Y.E. Penionzhkevich, Z. Podolyak, P. Roussel-Chomaz, M.G. Saint Laurent, H. Savajols, O. Sorlin, G. Sletten, D. Sohler, J. Timar, C. Timis, A. Yamamoto, Eur. Phys. J. A **20**, 95 (2004).

[17] Z. Elekes, Zs. Dombradi, R. Kanungo, H. Baba, Zs. Fulop, J. Gibelin, A. Horvath, E. Ideguchi, Y. Ichikawa, N. Iwasa, H. Iwasaki, S. Kanno, S. Kawai, Y. Kondo, T. Motobayashi, M. Notani, T. Ohnishi, A. Ozawa, H. Sakurai, S. Shimoura, E. Takeshita, S. Takeuchi, I. Tanihata, Y. Togano, C. Wu, Y. Yamaguchi, Y. Yanagisawa, A. Yoshida, K. Yoshida, Phys. Lett. **B614**, 174 (2005).

[18] Y. Kondo, T. Nakamura, Y. Satou, T. Matsumoto, N. Aoi, N. Endo, N. Fukuda, T. Gomi, Y. Hashimoto, M. Ishihara, S. Kawai, M. Kitayama, T. Kobayashi, Y. Matsuda,3 N. Matsui, T. Motobayashi, T. Nakabayashi, K. Ogata, T. Okumura, H.J. Ong, T.K. Onishi, H. Otsu, H. Sakurai, S. Shimoura, M. Shinohara, T. Sugimoto, S. Takeuchi, M. Tamaki, Y. Togano, and Y. Yanagisawa, Phys. Rev. C **79**, 014602 (2009).

[19] D. Suzuki, H. Iwasaki, H.J. Onga, N. Imai, H. Sakurai, T. Nakao, N. Aoi, H. Baba, S. Bishop, Y. Ichikawa, M. Ishihara, Y. Kondoc, T. Kubob, K. Kurita, T. Motobayashi, T. Nakamura, T. Okumura, T.K. Onishi, S. Ota, M.K. Suzuki, S. Takeuchi, Y. Toganod, Y. Yanagisawa, Phys. Lett. **B666**, 222, (2008).

[20] H.G. Bohlen, R. Kalpakchieva, W. von Oertzen, T.N. Massey, B. Gebauer, T. Kokalova, A.A. Ogloblin, Ch. Schulz, S. Thummerer, Nucl. Phys. **A738**, 333 (2004).

[21] E.K. Warburton and D.J. Millener, Phys. Rev. C **39**, 1120 (1989).

[22] R. Harkewicz, D.J. Morrissey, B.A. Brown, J.A. Nolen, Jr., N.A. Orr, B.M. Sherrill, J.S. Winfield, J.A. Winger, Phys. Rev. C **44**, 2365 (1991).

[23] K.W. Scheller, J. Görres, J.G. Ross, M. Wiescher, R. Harkewicz, D.J. Morrissey, B.M. Sherrill, M. Steiner, N.A. Orr, J.A. Winger, Phys. Rev C **49**, 46 (1994).

[24] G. Raimann, A. Ozawa, R.N. Boyd, F.R. Chloupek, M. Fujimaki, K. Kimura, T. Kobayashi, J.J. Kolata, S. Kubono, I. Tanihata, Y. Watanabe, and K. Yoshida, Phys. Rev C **53**, 453 (1996).

[25] N. Aoi, K. Yoneda, E. Ideguchi, T. Kishida, T. Nakamura, M. Notani, H. Sakurai, T. Teranishi, Y. Watanabe, H. Wu, A. Yoshida, H. Miyatake, Y. Yamamoto, H. Ogawa, S.S. Yamamoto, M. Ishihara, Phys. Rev. C **66**, 014301 (2002).

[26] K. Asahi, M. Ishihara, N. Inabe, T. Ichihara, T. Kubo, M. Adachi, H. Takahashi, M. Kouguchi, M. Fukuda, D. Mikolas, D.J. Morrissey, D. Beaumel, T. Shimoda, H. Miyatake, and N. Takahashi, Phys. Lett. **B251**, 488 (1990).

[27] H. Okuno, K. Asahi, H. Sato, H. Ueno, J. Kura, M. Adachi, T. Nakamura, T. Kubo, N. Inabe, A. Yoshida, T. Ichihara, Y. Kobayashi, Y. Ohkubo, M. Iwamoto, F. Ambe, T. Shimoda, H. Miyatake, N. Takahashi, J. Nakamura, D. Beaumel, D.J. Morrissey, W.-D. Schmidt-Ott, and M. Ishihara, Phys. Lett. **B335**, 29 (1994).

[28] H. Miyatake, H. Ueno, Y. Yamamoto, N. Aoi, K. Asahi, E. Ideguchi, M. Ishihara, H. Izumi, T. Kishida, T. Kishida, T. Kubo, S. Mitsuoka, Y. Mizoi, M. Notani, H. Ogawa, A. Ozawa, M. Sasaki, T. Shimoda, T. Shirakura, N. Takahashi, S. Tanimoto, K. Yoneda, Phys. Rev. C **67**, 014306 (2003).

[29] Y. Hirayama, T. Shimoda, H. Izumi, A. Hatakeyama, K.P. Jackson, C.D.P. Levy, H. Miyatake, M. Yagi, H. Yano, Phys. Lett. **B611**, 239 (2005).

[30] K. Kura, K. Tajiri, T. Shimoda, A. Odahara, T. Hori, M. Kazato, T. Masue, M. Suga, A. Takashima, T. Suzuki, T. Fukuchi, Y. Hirayama, N. Imai, H. Miyatake, M. Pearson, C.D.P. Levy, K.P. Jackson, Phys. Rev. C **85**, 034310 (2012).

[31] H. Ueno, K. Asahi, H. Izumi, K. Nagata, H. Ogawa, A. Yoshimi, H. Sato, M. Adachi, Y. Hori, K. Mochinaga, H. Okuno, N. Aoi, M. Ishihara, A. Yoshida, G. Liu, T. Kubo, N. Fukunishi, T. Shimoda, H. Miyatake, M. Sasaki, T. Shirakura, N. Takahashi, S. Mitsuoka, W.-D. Schmidt-Ott, Phys. Rev. C **53**, 2142 (1996).

[32] T. Kubo, M. Ishihara, N. Inabe, H. Kumagai, I. Tanihata, K. Yoshida, T. Nakamura,

H. Okuno, S. Shimoura, and K. Asahi, Nucl. Instrum. Methods B **70**, 309 (1992).

[33] K. Sugimoto, A. Mizouchi, K. Nakai and K. Matsuta, J. Phys. Soc. Japan **21**, 213 (1966).

[34] H. Ohm, W. Rudolph, and K.-L. Kratz, Nucl. Phys. **A274**, 45 (1976).

[35] R.A. Cecil, B.D. Anderson, and R. Madey, Nucl. Instrum. Methods Phys. Res. **161**, 439 (1979).

[36] P.M. Jones, L. Wei, F.A. Beck, P.A. Butler, T. Byrski, G. Duchêne, G. de France, F. Hannachi, G.D. Jones and B. Kharraja, Nucl. Instrum. Methods A **362**, 556 (1995).

[37] HAMATSU H6614-01

[38] A. Abragam, *The Principle of Nuclear Magnetism,* (Clarendon, Oxford, 1961).

[39] J.P. Dufour, R.Del Moral, F. Hubert, D. Jean, M.S. Pravikoff, A. Fleury, A.C. Mueller, K.-H. Schmidt, K. Summerer, E. Hanelt, J. Frehaut, M. Beau, G. Giraudet, Phys. Lett. **B206**, 195 (1988).

[40] P.L. Reeder, R.A. Warner, W.K. Hensley, D.J. Vieira, J.M. Wouters, Phys. Rev. C **44**, 1435 (1991).

[41] R. Brun, F. Carminati, CERN Application Software Group, GEANT3.2, CERN Program Library Writeup Report No. W5013 (1994).

[42] D.R. Tilley, Nucl. Phys. **A565**, 1 (1993).

[43] D.E. Alburger and D.J. Millener, Phys. Rev. C **20**, 1891 (1979).

[44] F. Ajzenberg-Selove, Nucl. Phys. **A523**, 1 (1991).

[45] H. Ueno, D. Kameda, G. Kijima, K. Asahi, A. Yoshimi, H. Miyoshi, K. Shimada, G. Kato, D. Nagae, S. Emori, T. Haseyama, H. Watanabe, M. Tsukui, Phys. Lett. B **615**, 186 (2005).

[46] H. Ogawa, K. Asahi, K. Sakai, T. Suzuki, H. Izumi, H. Miyoshi, M. Nagakura, K. Yogo, A. Goto, T. Suga, T. Honda, H. Ueno, Y. X. Watanabe, K. Yoneda, A. Yoshimi, N. Fukuda, Y. Kobayashi, A. Yoshida, T. Kubo, M. Ishihara, N. Imai, N. Aoi, W.-D. Schmidt-Ott, G. Neyens, S. Teughels, Phys. Rev. C **67**, 064308 (2003).

[47] H. Ogawa, K. Asahi, K. Sakai, A. Yoshimi, M. Tsuda, Y. Uchiyama, T. Suzuki, K. Suzuki, N. Kurokawa, M. Adachi, H. Izumi, H. Ueno, T. Shimoda, S. Tanimoto, N. Takahashi, W. -D. Schmidt-Ott, M. Schafer, S. Fukuda, A. Yoshida, M. Notani, T. Kubo, H. Okuno, H. Sato, N. Aoi, K. Yoneda, H. Iwasaki, N. Fukuda, N. Fukunishi, M. Ishihara, H. Miyatake, Phys. Lett. **B451**, 11 (1999).

[48] H. Izumi, K. Asahi, H. Ueno, H. Okuno, H. Sato, K. Nagata, Y. Hori, M. Adachi, N. Aoi,

A. Yoshida, G. Liu, N. Fukunishi, M. Ishihara, Phys. Lett. **B366**, 51 (1996).

[49] H. Okuno, K. Asahi, H. Ueno, H. Izumi, H. Sato, M. Adachi, T. Nakamura, T. Kubo, N. Inabe, A. Yoshida, N. Fukunishi, T. Shimoda, H. Miyatake, N. Takahashi, W.-D. Schmidt-Ott, M. Ishihara, Phys. Lett. **B354**, 41 (1995).

[50] B.A. Brown, A. Etchegoyen, and W.D.M. Rae, OXBASH, MSU Cyclotron Laboratory Report No. 524 (1986).

[51] E.K. Warburton and B.A. Brown, Phys. Rev. C **46**, 923 (1992).

[52] D.J. Millener and D. Kurath, Nucl. Phys. **A255**, 315 (1975).

[53] T.T.S. Kuo and G.E. Brown, Nucl. Phys. **85**, 40 (1966).

High-energy neutron
detector array (E_n = 0.5 ~ 10 MeV)

Ge detector

Helmholtz
coil

Pt stopper

NaI(Tl)
detectors

Low-energy neutron
detector array ($E_n \geq 0.01$ MeV)

^{17}B$\uparrow$ beam
from RIPS
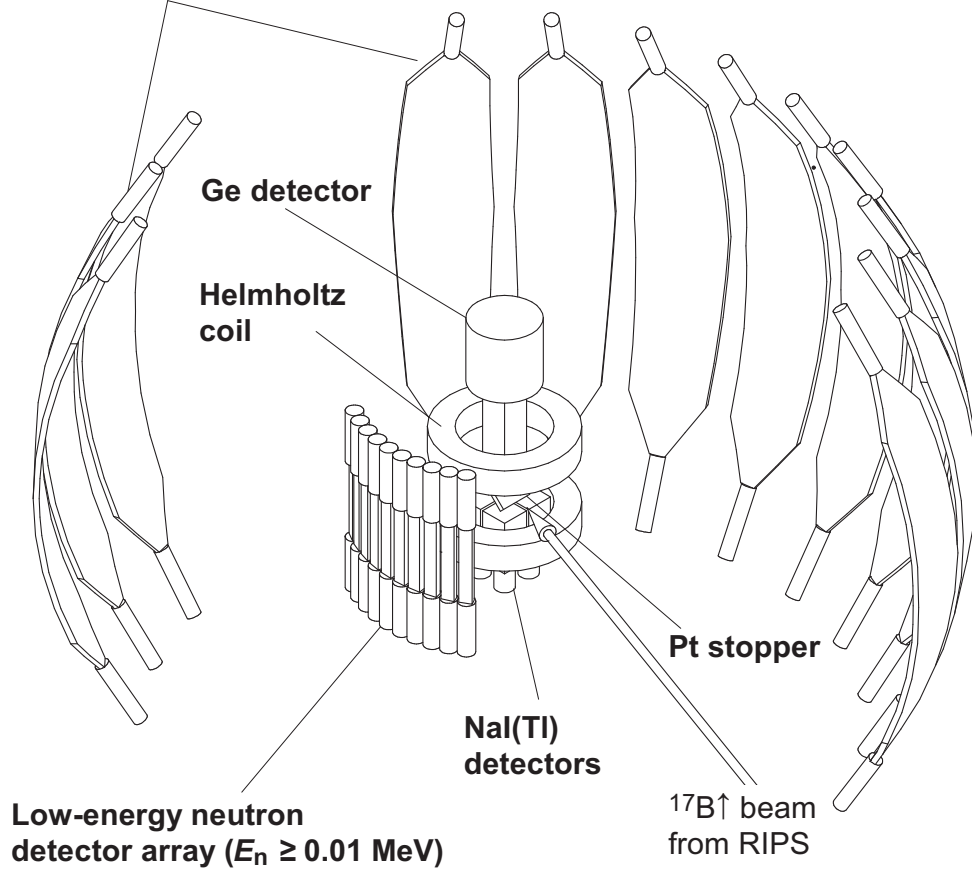
FIG. 1: Arrangement of the high-energy and low-energy neutron detector arrays.

Helmholtz coil

Plastic scintillator
(β-ray telescope)

Collimator

Pb shield

SSD

Ge detector

Stopper (Pt)

RF coil

Plastic scintillator
(β / γ identification)

Spin-polarized
^{17}B beam
from RIPS

Al absorber

Plastic scintillator
(RI beam counting)

NaI(Tl) x 4

0   100 mm
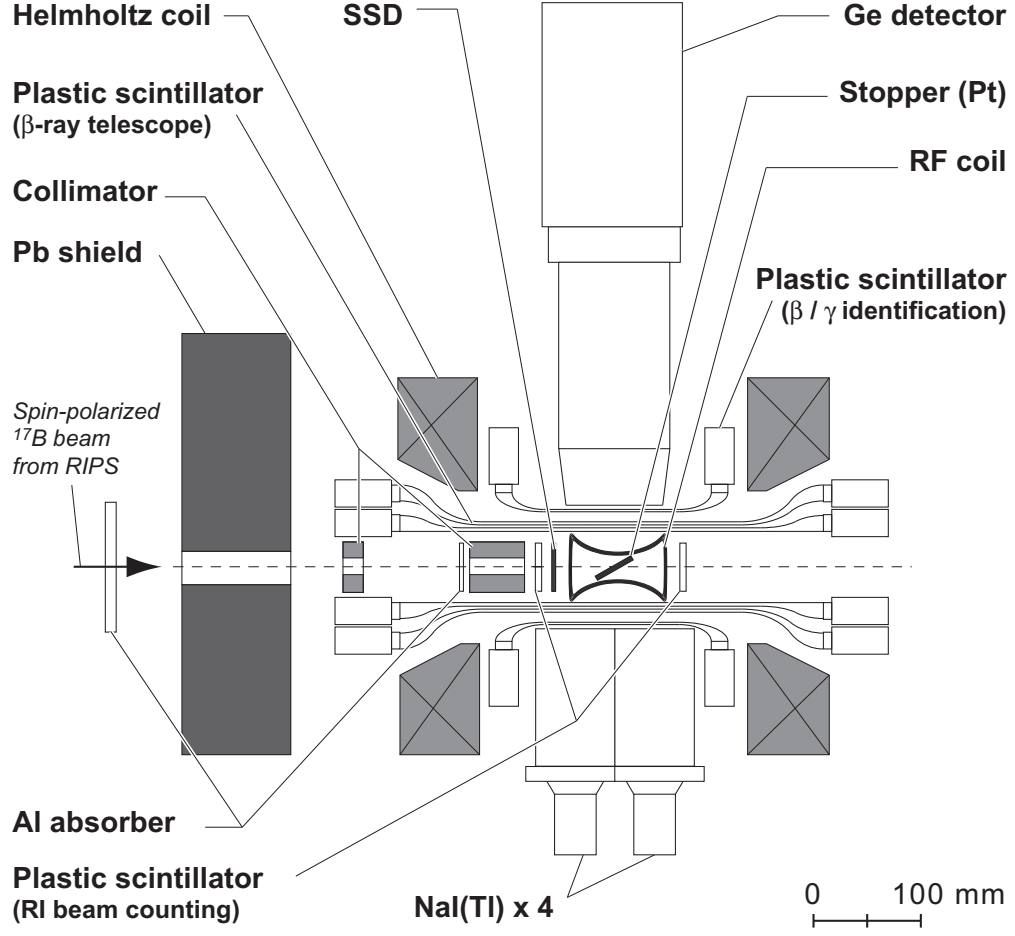
FIG. 2: Schematic layout of the setup around a Pt stopper, showing NaI(Tl) and Ge γ-ray detectors and a β-NMR system.
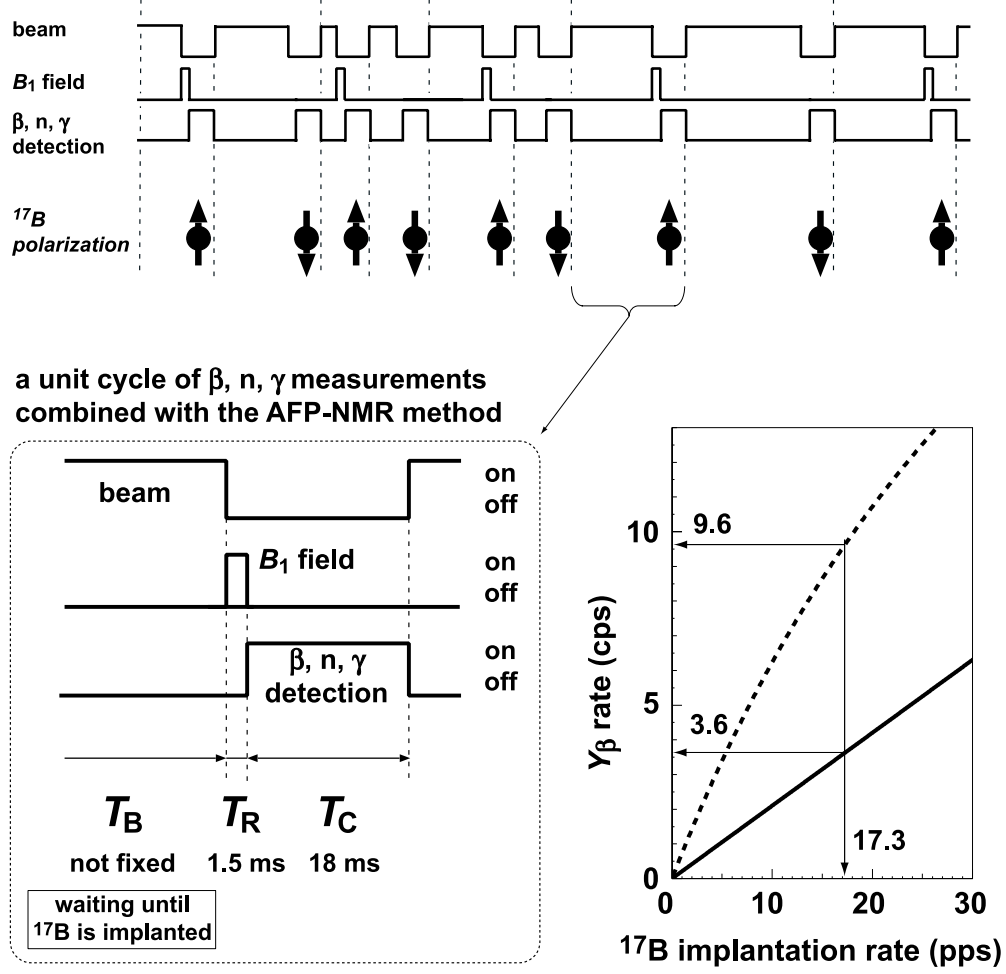
FIG. 3: Block diagram for the β-delayed neutron and/or γ ray measurement combined with the AFP-NMR technique. T_B, T_R, and T_C are the duration of the ^{17}B beam bombardment; the application of the B_1 field; and the β, neutron, and γ particle detection. T_R and T_C are fixed, while T_B is not fixed and remains open until a ^{17}B particle is implanted. The β decay rate Y_β, as the function of the ^{17}B implantation rate, of the new *beam waiting* mode was compared with that of the fixed beam-on/off cycle mode. For details, see the text.
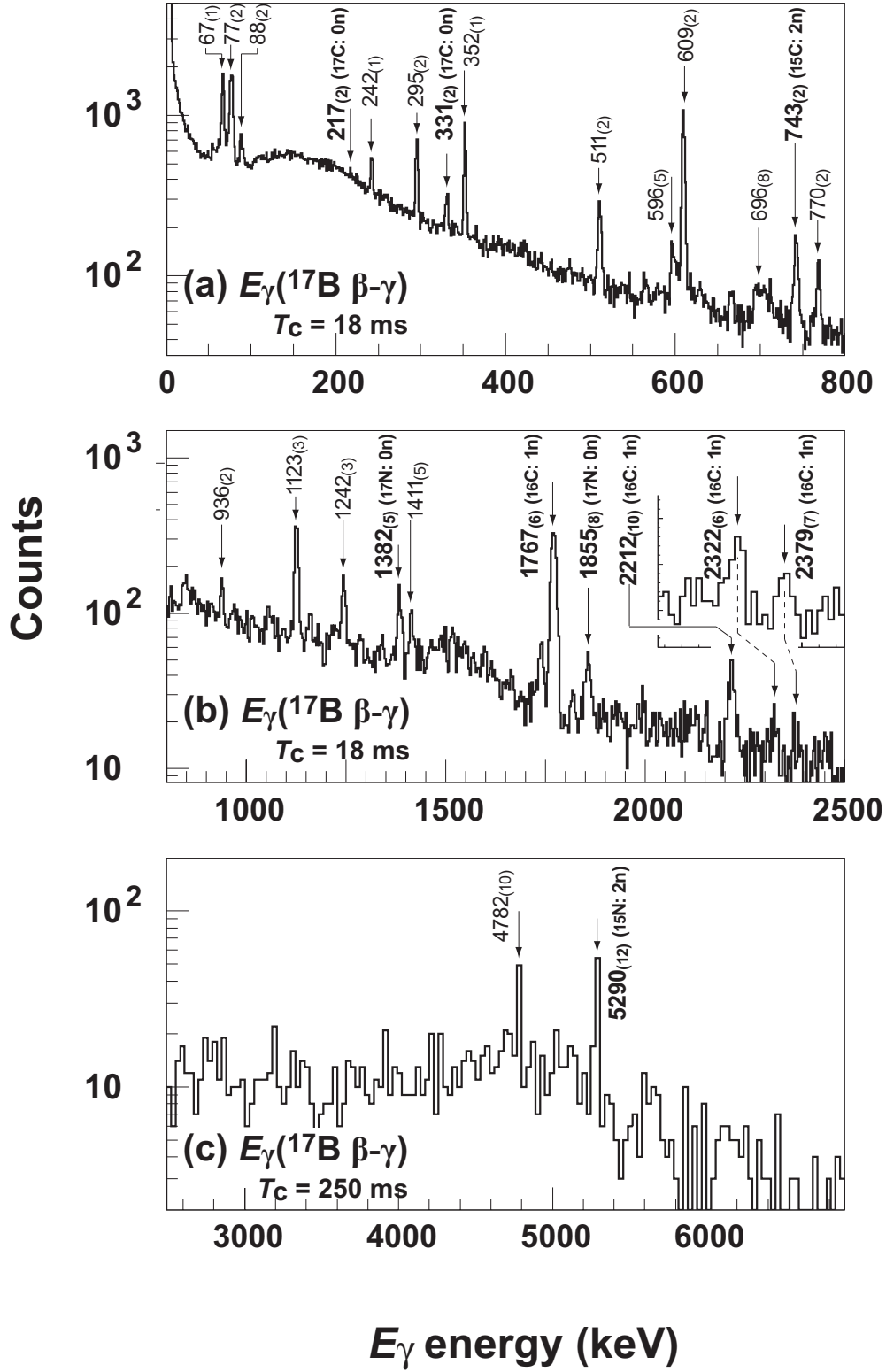
FIG. 4: γ-Ray energy spectra obtained with the Ge detector in coincidence with the β ray. The spectra were obtained with the counting periods T_C of (a) and (b) 18 ms and (c) 250 ms.
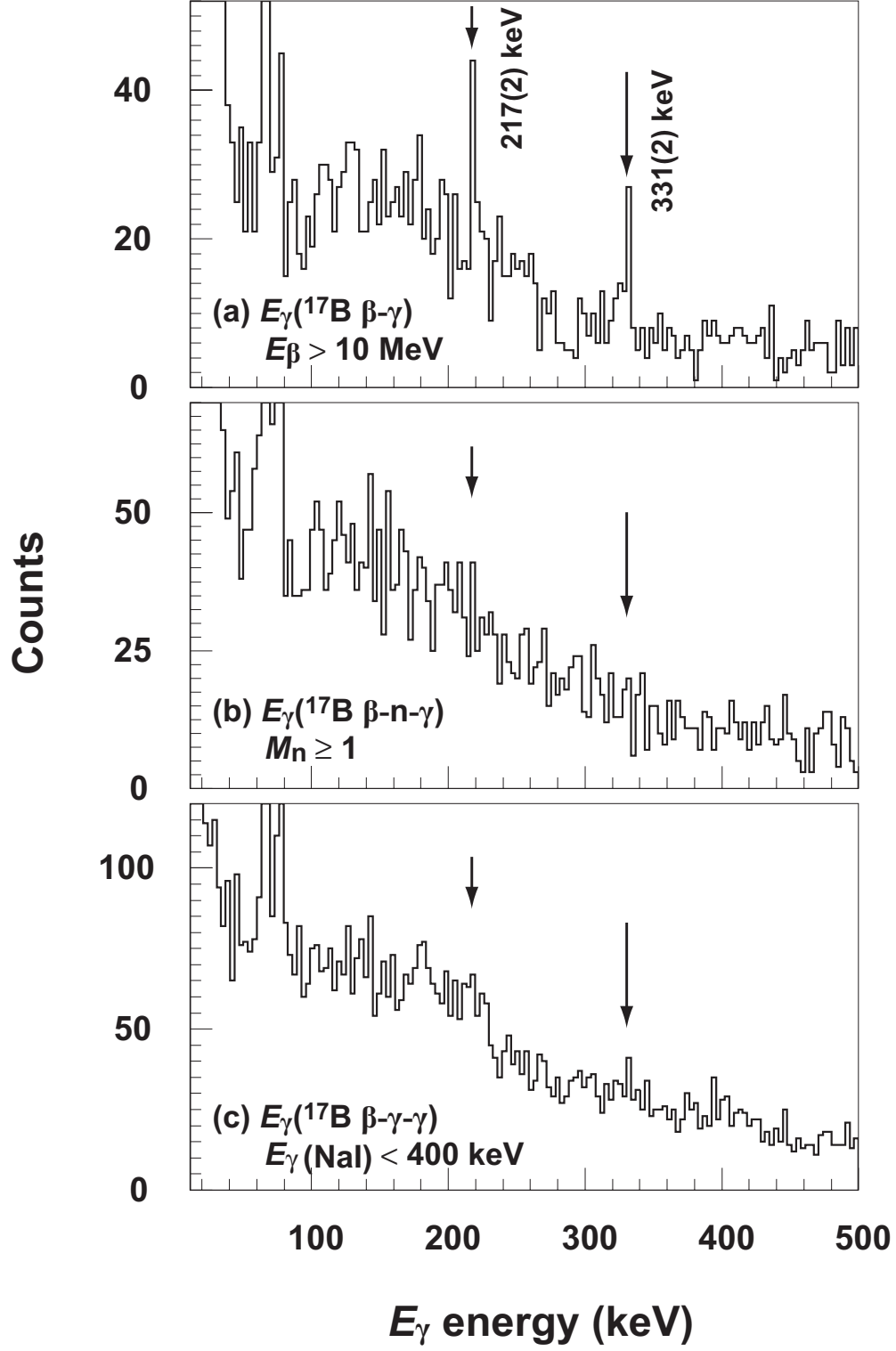
FIG. 5: Obtained γ-ray energy spectra measured with the Ge detector by gating with (a) β-ray energies $E_\beta > 10$ MeV, (b) neutron multiplicity $M_n \geq 1$, and (c) γ-ray energy $E_\gamma < 400$ keV measured with NaI(Tl) detectors.
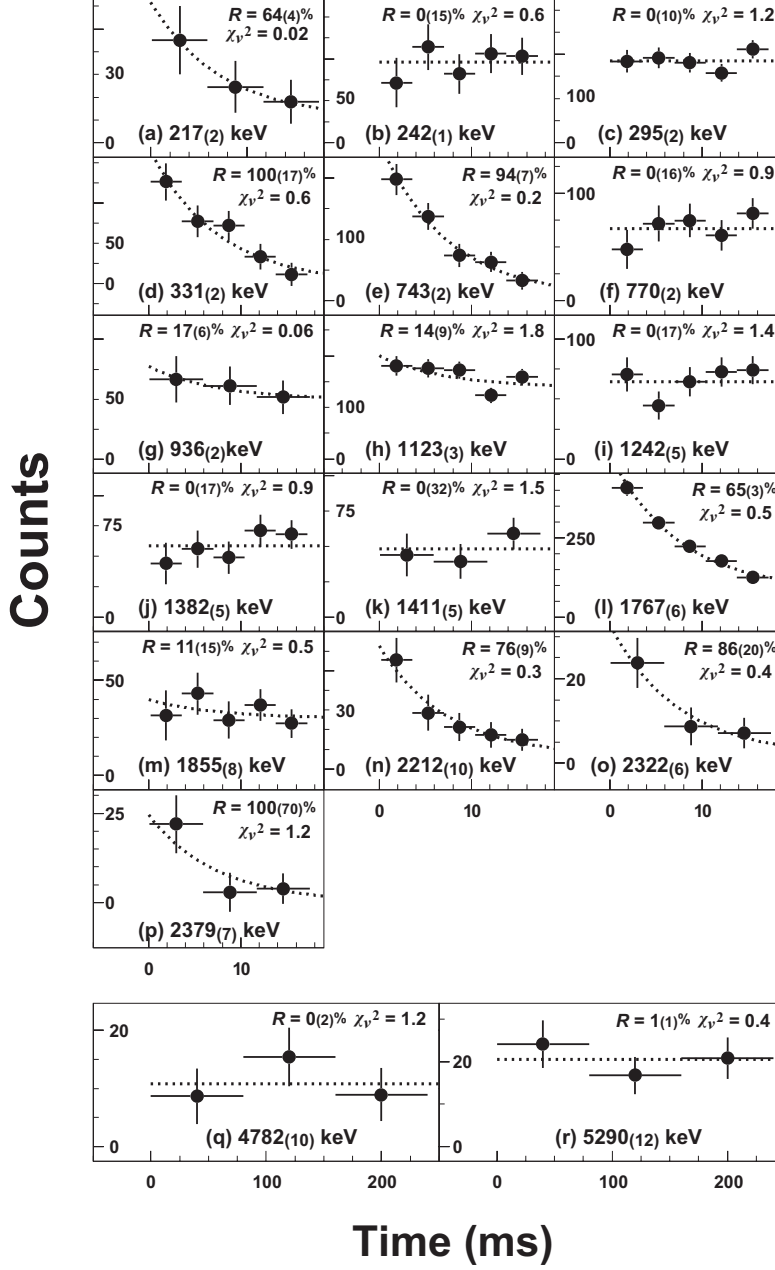
FIG. 6: Time evolution of the photo-peak counts of the observed β-γ lines measured with the Ge detector in the ^{17}B β decay. The vertical bar shows the statistical error, and the horizontal bar represents the time-slice window. The dotted line/curve shows the result of the χ^2-fitting analysis using an exponential function with the known halflife of ^{17}B, $t_{1/2} = 5.08(5)$ ms, plus a constant is used. Values R indicated in each panel shows the ratio of the exponential component to the total counts. The spectrum of (a) 217(2)-keV is obtained for an additional coincidence with a β ray having $E_\beta > 10$ MeV measured with the NaI(Tl) detector. Further, the spectra (q) and (r) are obtained with a measurement conducted separately by expanding T_C to 250 ms for investigating components with a long lifetime.
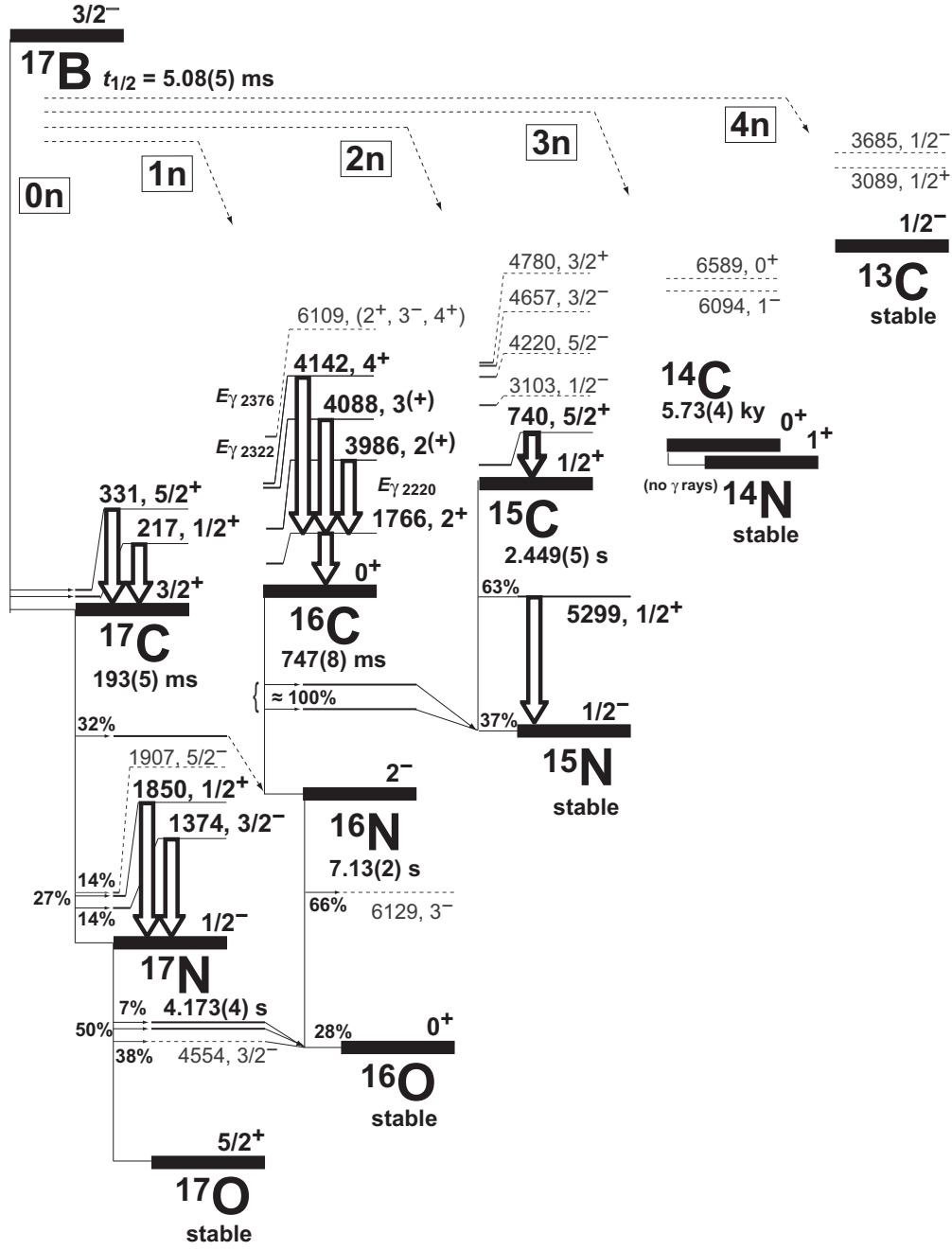
FIG. 7: Observed γ lines in the decay chain initiated by the ^{17}B β decay. The observed and identified γ lines are shown by open arrows.
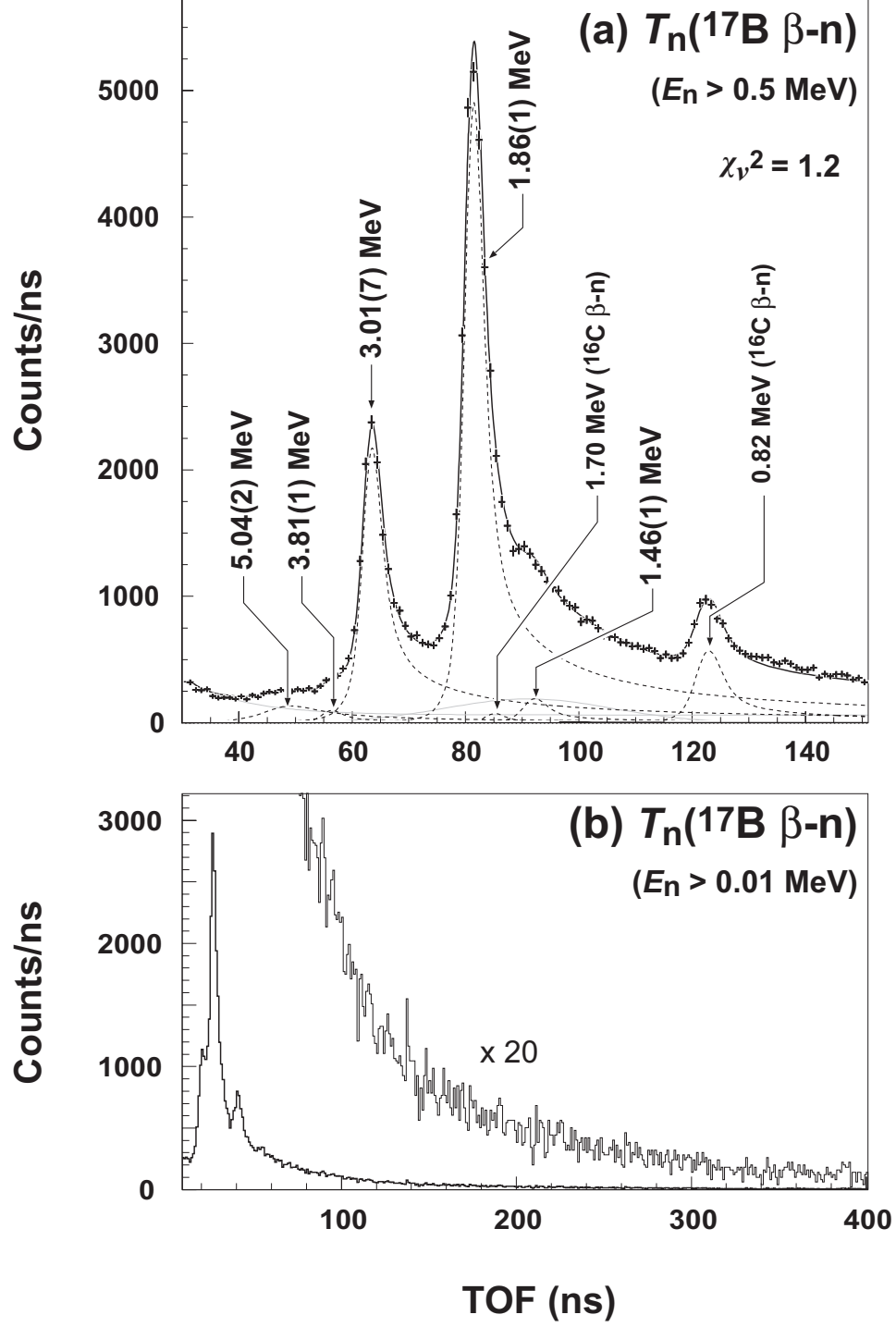
FIG. 8: TOF spectra obtained for the β-delayed neutrons emitted in the ^{17}B β decay with (a) high-energy and (b) low-energy neutron detector arrays. The solid curve shown in panel (a) is the result of a least χ^2-fitting analysis The decomposed components are represented by dashed curves.
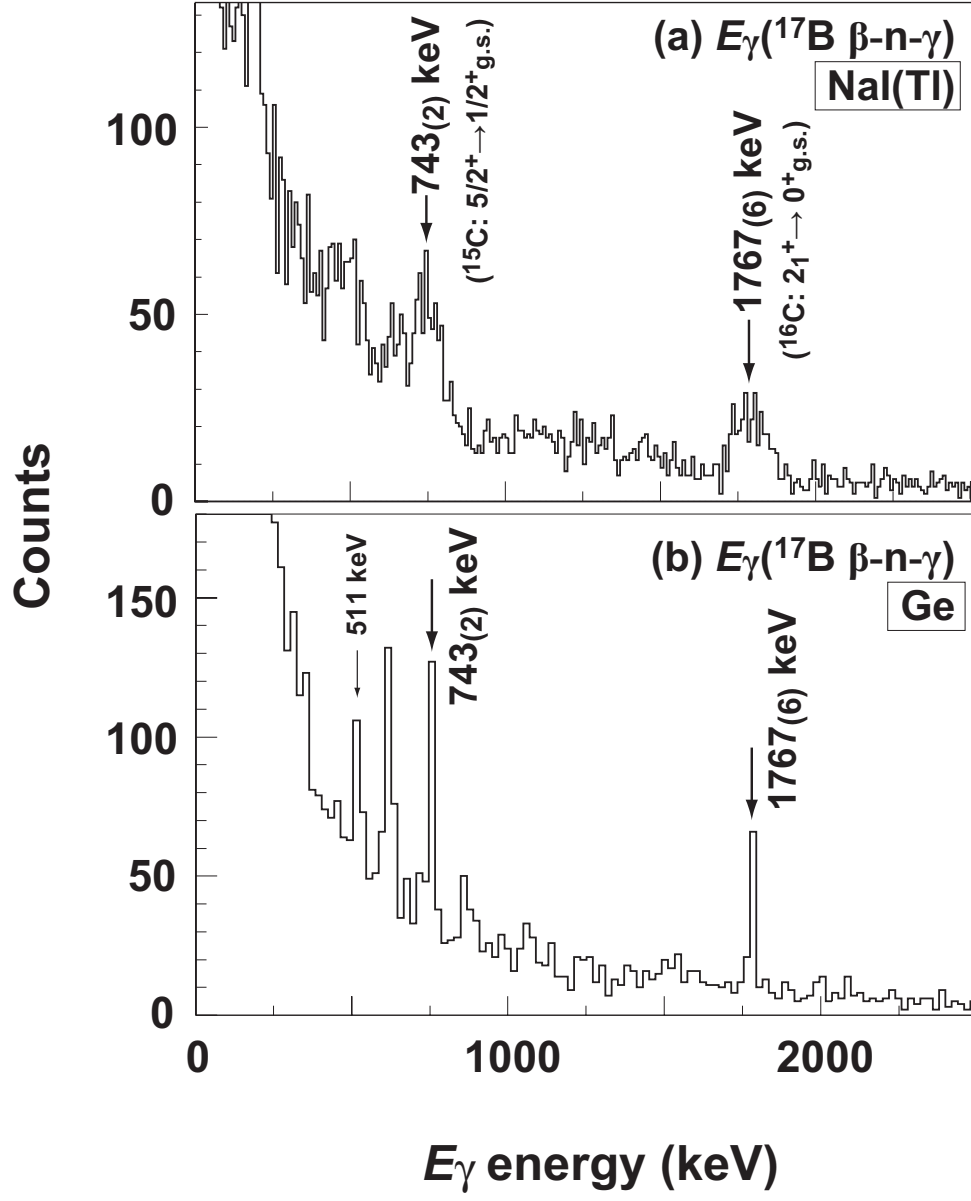
40

FIG. 9: Obtained γ-ray energy spectra with (a) NaI(Tl) detectors and (b) the Ge detector in coincidence with β-delayed neutrons with multiplicity $M_n = 1$.
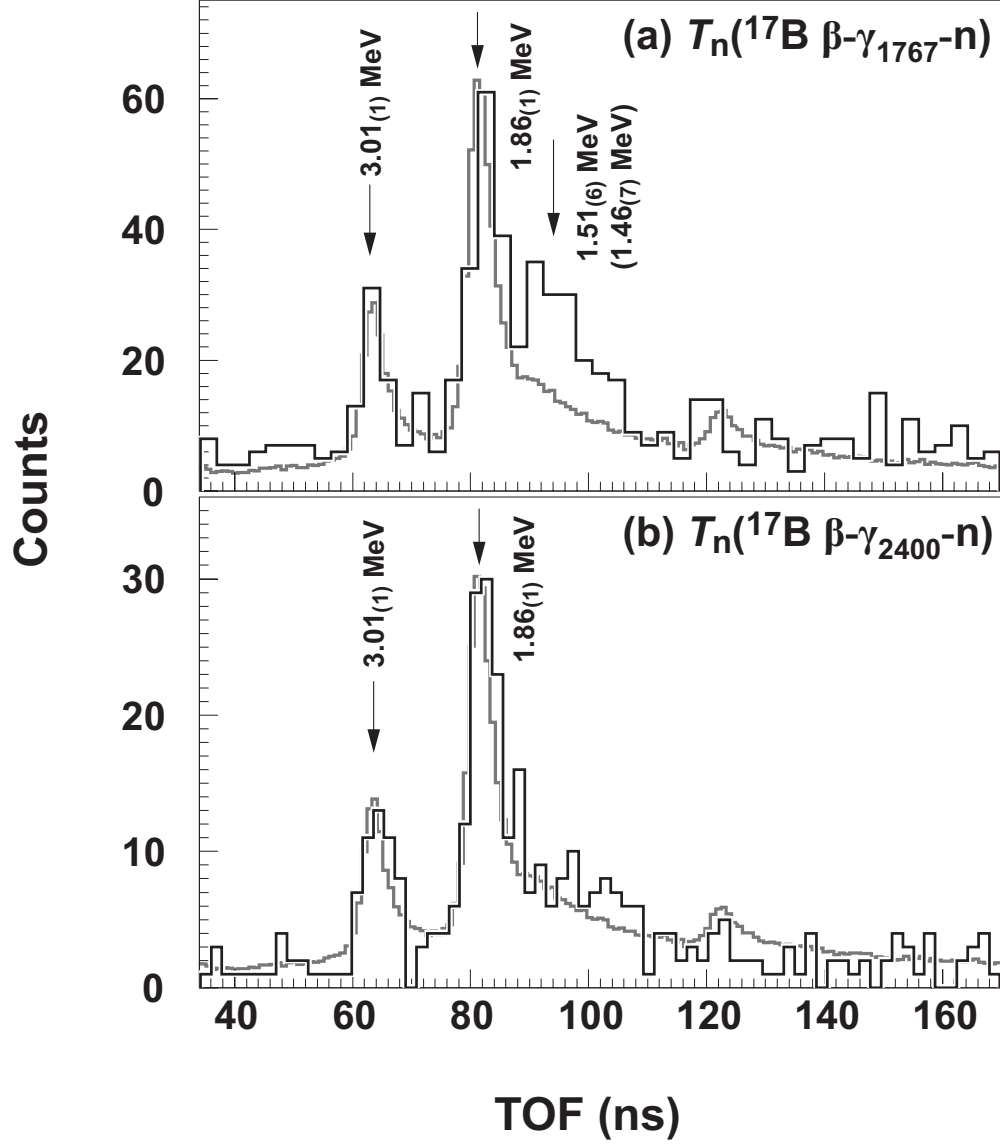
FIG. 10: TOF spectrum obtained with the neutron detector array in coincidence with a 1767(6)-keV γ peak observed with NaI(Tl) detectors.
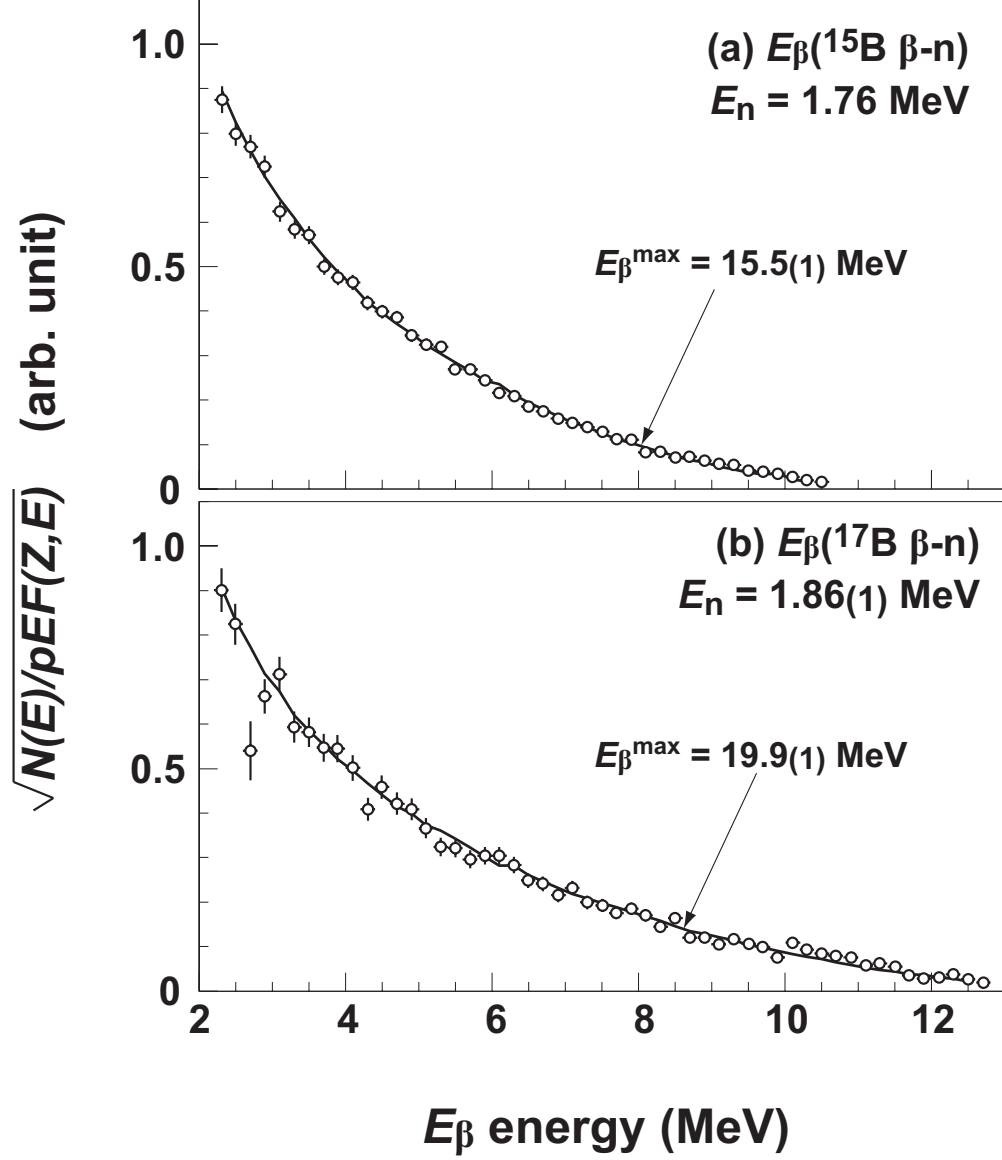
FIG. 11: β-Ray energy spectra (i.e., Kurie plot) measured with NaI(Tl) detectors in coincidence with (a) the 1.86(1)-MeV β-delayed neutrons in the ^{17}B β decay and (b) 1.76-MeV β-delayed neutrons in the ^{15}B β decay. Solid curves show the result of GEANT simulations, in which the end-point energies $E_\beta^{\max}$ = 19.7(1) MeV and 17.9(2) MeV were deduced, respectively. For comparison with the simulation results, β-ray yields are normalized to unity at $E_\beta = 2$ MeV.
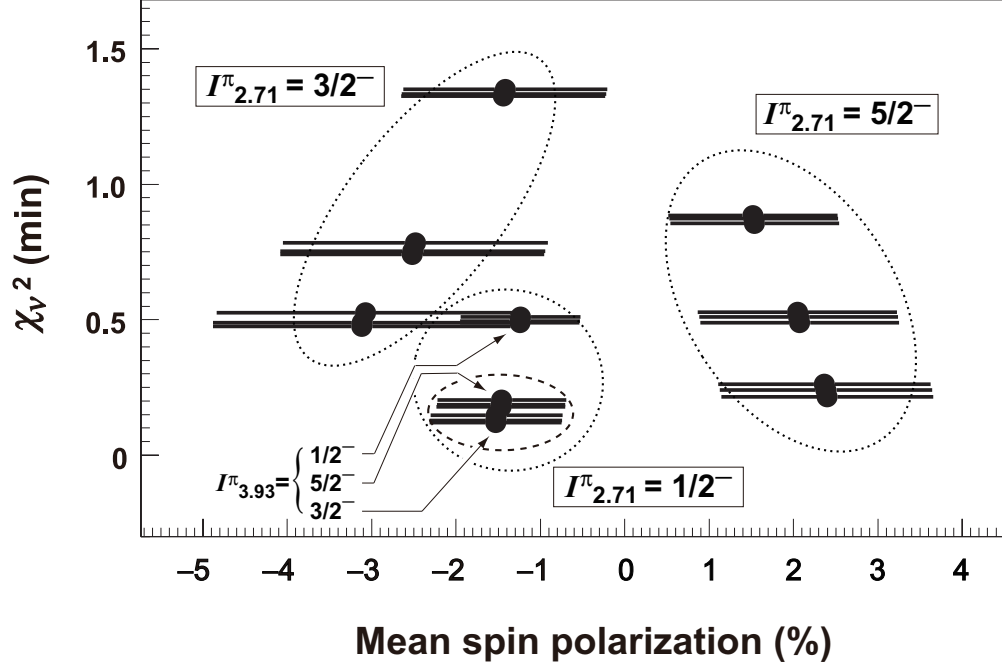
FIG. 12: Values of χ^2_ν plotted as a function of the mean spin polarization calculated for all possible sets of A_β values in the ^{17}B β-decay transition to the observed levels in ^{17}C at $E_x = 2.71(2)$, 3.93(2), and 4.05(2) MeV. Classification according to the I^π for $E_n = 2.71(2)$ MeV is indicated by dotted ellipses. The dashed ellipse shows the most probable sets of the A_β allocation.
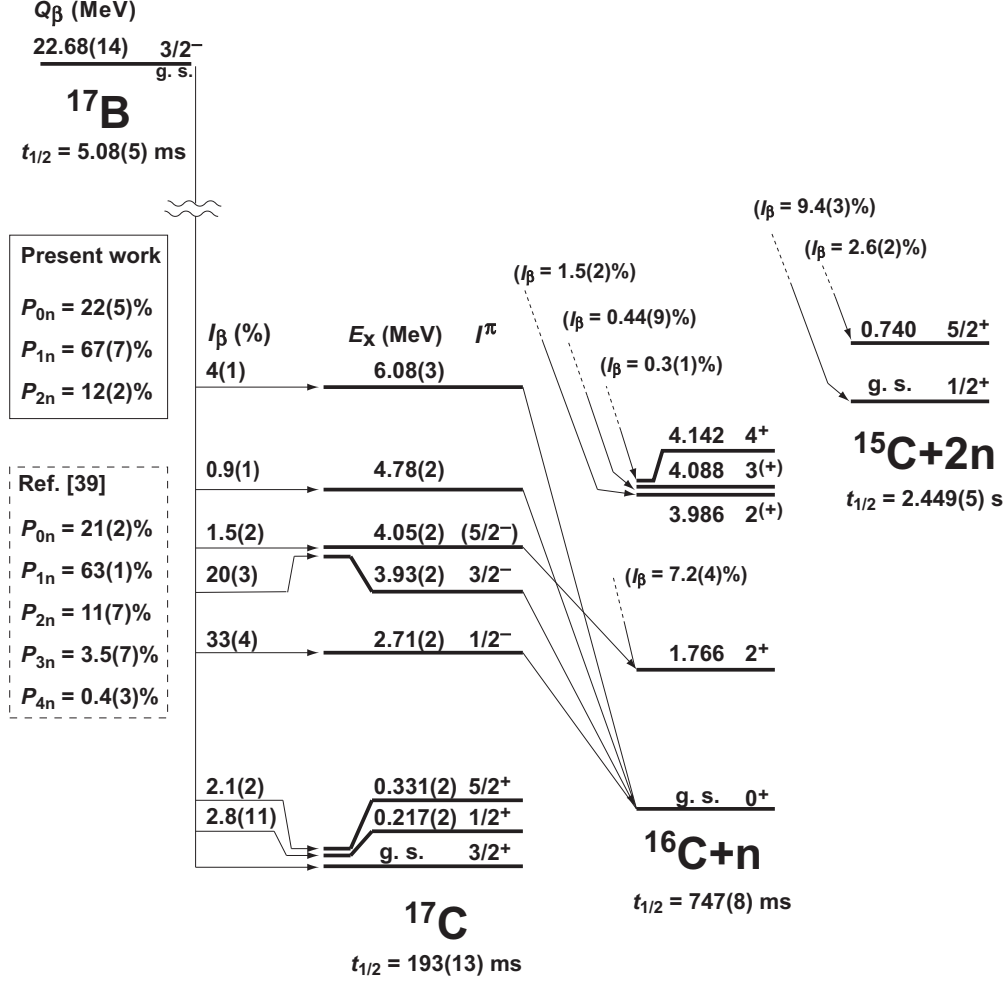
FIG. 13: Decay scheme of ^{17}B constructed in the present work. Unassigned levels $E_\mathrm{x} = 4.78(2)$ and 6.08(3) MeV are also shown.
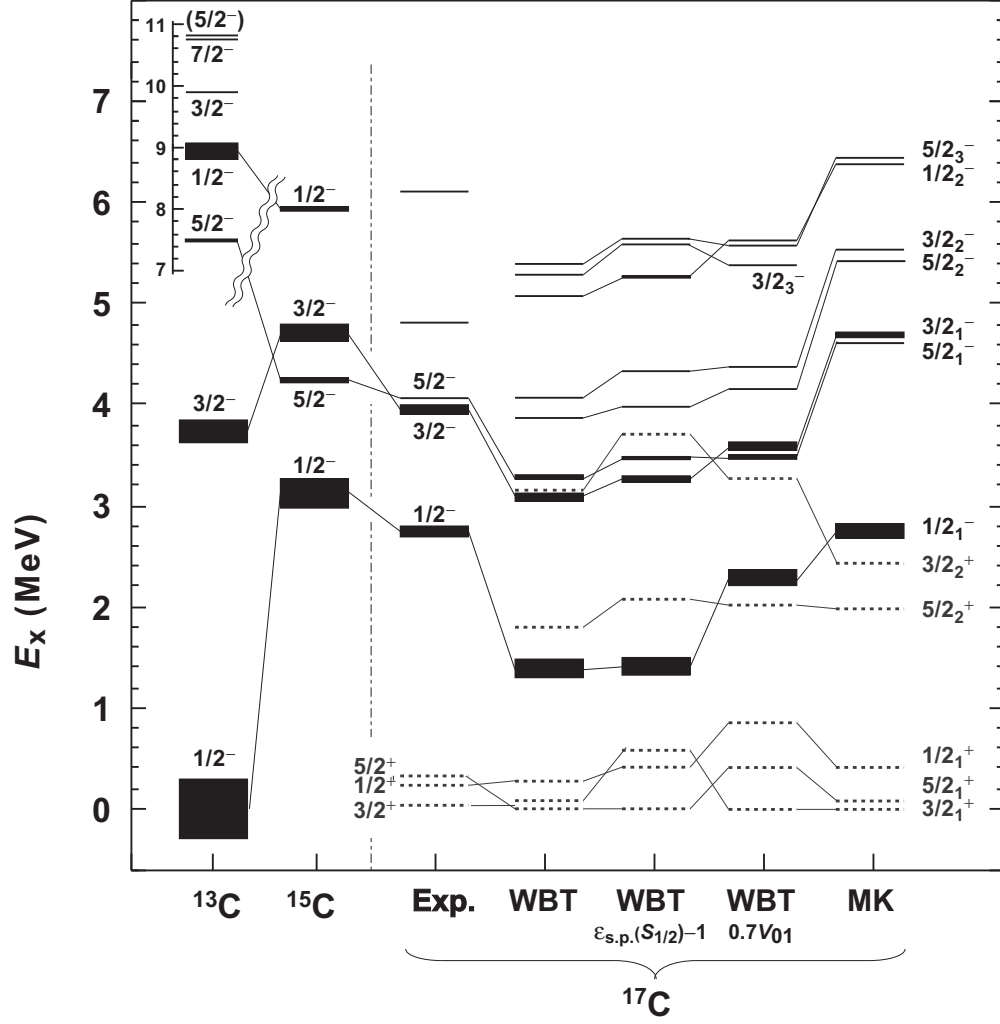
FIG. 14: Comparison of the obtained β-decay feeding excited states in ^{17}C with shell-model calculations, with positive and negative parity states indicated by dashed and solid lines, respectively. The negative-parity states in ^{13}C and ^{15}C are also shown.

TABLE I: Energies of the γ-ray observed as a peak in the β-γ coincidence measurements with ^{17}B and ^{17}N gbeams below the ^{17}C neutron-threshold energy $S_\mathrm{n} = 0.729(18)$ MeV, obtained using the Ge detector, together with those observed without a beam. Circles are used to indicate that they were observed in each measurement. Possible γ-ray origins are listed together in the last column, provided their energies agree with the experimental values.

E_γ (keV)	no beam	^{17}N β-γ	^{17}B β-γ	possible background sources	(keV)
67(1)	×	○	○	$\mathrm{KX}_{\alpha1}(\mathrm{Pt})$	66.8
				$^{73\mathrm{m}}\mathrm{Ge}$	66.6
77(2)	○	○	○	$\mathrm{KX}_{\alpha1}(\mathrm{Pb})$	75.0
				$\mathrm{KX}_{\beta1}(\mathrm{Pt})$	75.7
				$\mathrm{KX}_{\alpha1}(\mathrm{Bi})$	77.1
88(2)	×	×	○	$\mathrm{KX}_{\beta1}(\mathrm{Pb})$	87.3
217(2)	×	×	○	$(^{228}\mathrm{Ac})$	(216.0)
242(1)	○	×	○	$^{212}\mathrm{Pb}$	238.6
				$^{224}\mathrm{Ra}$	241.0
				$^{214}\mathrm{Pb}$	242.0
295(2)	×	×	○	$(^{214}\mathrm{Pb})$	(295.2)
331(2)	×	×	○	$(^{228}\mathrm{Ac})$	(328.0)
352(1)	○	○	○	$^{214}\mathrm{Pb}$	351.9
511(2)	○	○	○	annihilation	511.0
596(5)	×	○	○	$^{73}\mathrm{Ge}(\mathrm{n},\gamma)$	596.4
				$^{74}\mathrm{Ge}(\mathrm{n},\mathrm{n}'\gamma)$	
609(2)	○	○	○	$^{214}\mathrm{Bi}$	609.3
696(8)	×	○	○	$^{72}\mathrm{Ge}(\mathrm{n},\mathrm{n}'\gamma)$	693

TABLE II: Properties of β-γ rays observed in the ^{17}B β decay. This table lists the γ transition energies (E_γ), decay modes classified with the multiplicity of β-n emission, γ-ray emitter, level energies ($E_\mathrm{x}{}^\gamma$) in the γ emitter, level energies ($E_\mathrm{x}(^{17}\mathrm{C})$) in ^{17}C, γ- and β-ray intensities per ^{17}B decay (I_γ and I_β), and $\log ft$ values. For obtaining the I_β value at $E_\gamma = 1767(6)$ keV, the intensities of the cascade decay from 2212(10), 2322(6), and 2379(7) keV were subtracted.

E_γ (keV)	decay mode	γ emitter	$E_\mathrm{x}{}^\gamma$ (keV)	$E_\mathrm{x}(^{17}\mathrm{C})$ (keV)	I_γ (%)	I_β (%)	$\log ft$
217(2)	β(0n)	^{17}C	217(2)	217(2)	2.8(11)	2.8(11)	6.1(2)
331(2)	β(0n)	^{17}C	331(2)	331(2)	2.1(2)	2.1(2)	6.22(5)
740(2)	β(2n)	^{15}C	740.0(15)	not identified	2.6(2)	2.6(2)	
1767(6)	β(1n)	^{16}C	1766(10)	4050(20)	9.4(3)	7.2(4)	5.29(3)
1382(5)	β(0n)-β(^{17}C)	^{17}N	1373.8(3)	–	5.9(6)	–	
1855(8)	β(0n)-β(^{17}C)	^{17}N	1849.5(3)	–	4.5(6)	–	
2212(10)	β(1n)	^{16}C	3986(7)	not identified	1.5(2)	1.5(2)	
2322(6)	β(1n)	^{16}C	4088(7)	not identified	0.44(9)	0.44(9)	
2379(7)	β(1n)	^{16}C	4142(7)	not identified	0.3(1)	0.3(1)	
5290(12)	β(2n)-β(^{15}C)	^{15}N	5298.822(14)	–	7.5(11)	–	

TABLE III: Levels in ^{17}C observed in the 1n-decay channel following the β decay of ^{17}B, which are listed along with the excitation energies E_x for ^{17}C and the neutron-kinetic energies E_n, from which the E_x values are converted. The inconclusive levels are indicated by { }. Determined transition strengths I_β and values of $\log ft$ for the ^{17}C levels are also listed. For details, see the text.

E_n (MeV)	E_x (MeV)	width (MeV)	I_β (%)	$\log ft$	B(GT)	$A_\beta P$ (%)	A_β	$2I^\pi$ (χ^2_ν analysis)	$2I^\pi$ (end result)
{ 5.04(2)	6.08(3)	2.5(7)	4(1)	5.3(1)	0.021(3)				}
{ 3.81(1)	4.78(2)	0.3(3)	0.9(1)	6.1(1)	0.003(1)				}
1.46(1)	4.05(2)	0.06(6)	1.5(2)	6.0(1)	0.004(1)	+6(23)	−4(15)	$(1^-, 3^-, 5^-)$	(5^-)
3.01(1)	3.93(2)	0.16(4)	20(3)	4.9(1)	0.05(1)	−0.1(15)	+0.04(99)	$(3^-, 5^-)$	3^-
1.86(1)	2.71(2)	0.04(1)	33(4)	4.8(1)	0.07(1)	+1.6(8)	−1.0(5)	1^-	1^-